The High Latitude Ionosphere-Magnetosphere Transition Region: Simulation and Data Comparison

NASA GRANT: NAGW-3470

Progress Report: March 1994—February 1995

Principal Investigator: **Gordon R. Wilson**
/Institution   Department of Physics/Center for Space Plasma and
                          Aeronomic Research
                          The University of Alabama in Huntsville
                          Huntsville, AL 35899

Co-Investigator: **James L. Horwitz**
/Institution   Department of Physics/Center for Space Plasma and
                          Aeronomic Research
                          The University of Alabama in Huntsville
                          Huntsville, AL 35899

Collaborator: **Thomas E. Moore (NASA/MSFC)**

Summary of Second Year's Activities

Below is a brief description of the major activities for this grant during the last year. Reprints of two papers (one published and the other in press) describing some of this work are attached to this report.

1. Development of a 200 km—1 Re, O^+ H^+ Model. We have modified the basic IMTR model so that it deals with a region from 200 km to 1 Re altitude and models both the O^+ and H^+ ions. All of the O^+–neutral chemistry previously discussed has been included as well as the accidentally resonant charge exchange reaction with couples the O^+ and H^+ ions. Currently the electrons are included as a massless neutralizing fluid whose density and drift speed match that of the ions and whose temperature profile is given.

2. Extension of the **E** × **B** *convection heating study to include centrifugal effects.* The improved model was used to extend the **E** × **B** convection heating study [*Wilson*, 1994] to higher altitudes so that the consequences of the centrifugal force could be determined. Results of this study were presented at the October 1994 Huntsville workshop on Coupling of Micro and Mesoscale Processes in Space Plasma Transport and have been submited for publication in the proceedings. These results were also presented at the AGU 1994 fall meeting in San Francisco.

3. Study of electron precipitation effects. The model mentioned in *1* above was used to study the effect of energetic electron precipitation. To include the energetic electrons we used a two stream electron code developed by Phil Richards. At present the model only includes the ionization effects of these electrons and not there effect on thermal electron temperature. Preliminary results of this study were presented at the October 1994 Huntsville workshop and at the 1994 AGU fall meeting in San Francisco.

4. Study of wave heating of O^+. During 1994 a graduate student (D. Gristina) began a study of the consequences of O^+ wave driven heating that occurs at altitudes where collisions are important. The waves are produced by precipitating electrons with unstable velocity distributions. All the calculations done so far have been local, ignoring the effects of transport. Results of this study were presented at the 1994 AGU fall meeting in San Francisco.

5. Polar wind acceleration region study. During 1994 we also made progress in data/model comparison study of the polar wind acceleration region. During the summer of '94 a visiting undergraduate student worked with the RIMS data to find a way to sort H^+ spin curves by type, principally in terms of the degree of skewing. We now know how common the highly skewed spin curves are. Earlier in the year we performed a number of simulation runs for comparison with this data. The runs were matched to the conditions of the data as much as possible. We found that the model can produced H^+ velocity distributions which give skewed spin curves, when passed through a RIMS instrument simulation filter, but the data often shows more skewing than the current model can explain. Results of this study were presented at the 1994 AGU spring meeting in Baltimore and at the COSPAR meeting in Hamburg.

Plans for the Third Year

During the coming year we plan to pursue four major areas as described below.

1. Wave heating induced transport of O^+. During the coming year D. Gristina will use the transport model described in *1* above to study the consequences for O^+ transport of wave heating. This will involve modifying the model to include the heating algorithm developed for the local calculations discussed in *4.* above. Parameters used for this study will primarily be those appropriate to the TOPAZ III rocket flight. This work will constitute Mr. Gristina's masters thesis.

2. Proton aurora study. One of the main areas discussed in the original proposal which has not been addressed yet is the consequences of energetic ion precipitation for the IMTR. We plan, in the next year, to study the effect of proton precipitation, particularly the means by which energetic protons could transfer energy to the ionospheric ions. Such energy transfer could occur through collisions or plasma instabilities.

3. Finish study of energetic electron precipitation. The energetic electron precipitation study will be continued by upgrading the model through the addition of a more sophisticated electron description which solves the electron energy equations using expression for the electron heat flow. This will allow us to vary the electron temperature with time and altitude to see how ion outflow is affect by this aspect of the energetic electron precipitation process.

4. Finish polar cap data-model comparison study. The next step in this study will be a statistical analysis of the different types of RIMS spin curves to determine the dependence on various geophysical parameters such as altitude, latitude, season, $F_{10.7}$, Kp, etc. These results will hopefully serve as a guide for additional simulations that might explain the more dramatically skewed spin curves. In addition we will study the possibility that a streaming instabilities between the H^+ and O^+ ions in the acceleration region might account for the more skewed cases. Recent work done by a collaborator here has suggested a way where the microscale effects of the instability can be included in the mesoscale model that is used here.

Papers Published

Wilson, G. R., Kinetic modeling of O^+ upflows resulting from $\mathbf{E} \times \mathbf{B}$ convection heating in the high latitude F region ionosphere, *J. Geophys. Res.*, *99*, 17453, 1994.

Papers Submitted

Wilson, G. R., B. L. Giles, and M. O. Chandler, Collisional to collisionless ion outflow at the ionosphere-magnetosphere interface, *Adv. Space Res.*, in press, 1995.

Wilson, G. R., The Consequences of Coulomb collisions for space plasma transport, in *Coupling of Micro and Mesoscale Processes in Space Plasma Transport*, AGU monograph series, eds. J. L. Horwitz, N. Singh, and J. Burch, 1995.

Ho, C.-W., J. L. Horwitz, G. R. Wilson, and D. G. Brown, Field-aligned transport and velocity distributions of H^+ and O^+ ions due to large $\mathbf{E} \times \mathbf{B}$ convection in the high latitude ionosphere, in *Coupling of Micro and Mesoscale Processes in Space Plasma Transport*, AGU monograph series, eds. J. L. Horwitz, N. Singh, and J. Burch, 1995.

COLLISIONAL TO COLLISIONLESS ION OUTFLOW AT THE IONOSPHERE-MAGNETOSPHERE INTERFACE

G. R. Wilson

Department of Physics and Center for Space Plasma and Aeronomic Research, University of Alabama in Huntsville, Huntsville, AL 35899, USA

B. L. Giles and M. O. Chandler

Space Science Laboratory, Marshall Space Flight Center, Huntsville, AL 35812, USA

ABSTRACT

Simple calculations show that ions in the ionosphere are collision dominated while ions in low density regions of the magnetosphere are collisionless. For the free outflow of light ions such as H^+ and He^+, this collisional-collisionless transition occurs in the region where the ions are accelerated by the charge separation electric field resulting from the steep gradient in the O^+ density. In this case, specific distortions of the light ion velocity distributions are produced that significantly alter ion temperatures and heat flows. The types of nonMaxwellian velocity distributions seen are distributions with downward suprathermal tails, inverted bowl shaped distributions, and highly skewed distributions with large parallel or perpendicular heat flows. In addition, distributions with multiple peaks or one peak and an extended plateau also develop under some conditions. These various distributions are the result of relative flow between species, the v^{-4} dependence of the Coulomb collision cross section, and altitude distributed sources of the ions. This paper presents results of studies of the evolution of the ion velocity distribution in the transition region done with a collisional semikinetic model combining the effects of large scale forces and field-aligned transport with the effects of ion-neutral and ion-ion collisions. Comparison of these results with data from the RIMS instrument on the DE 1 spacecraft suggest that these distributions have been seen and that additional processes, such as downward electric fields, may frequently be present on polar cap field lines.

INTRODUCTION

It has been known for several decades that the light ions H^+ and He^+ can freely escape from the high latitude ionosphere on field lines open to low pressure regions. Numerous studies of the polar wind using a variety of different models (moment based and kinetic) have been performed during this time /1/. Some of the basic predictions of the models have been confirmed by direct observation /2/ (and references therein).

One difficult aspect of polar wind study is understanding how the source of ions in the collision dominated ionosphere physically couples to the high speed flow region at high altitudes. This requires a knowledge of how ion flow develops while the ions are making a transition between collision dominated and collisionless regimes. To study this requires a model which is valid in both regimes. The first efforts to accomplish this were by Lemaire /3/ who combined a hydrodynamic model for the low altitude collisional region with a kinetic model for the high altitude collisionless region. A solution was obtained by matching density and velocity moments at the point where the two models were joined. Since that time more sophisticated generalized transport models that can span the collisional to collisionless transition have been developed /4,5,6/.

Because the moment based models place restrictions on the form of the velocity distribution, a kinetic model is needed to understand how the velocity distribution evolves through the transition region. Several recent efforts have been made in this direction /7,8/ inspired by the Monte Carlo calculations of Barakat and Lemaire /9/. Each of these models treats the collision process as a

random scattering event affecting ion simulation particles as they flow along field lines subject to the gravitational, magnetic mirror and ambipolar electric forces. In our model /7/ the Coulomb collision algorithm of Takizuka and Abe /10/ is used to simulated the effects of Coulomb collisions. This technique conserves momentum and energy and gives correct stopping, energy exchange and deflection frequencies for the Coulomb collision.

In this paper we present the results of recent calculations with the semikinetic transition region model for the outflow of H^+ and He^+ ions in the polar cap in the presence of O^+ whose characteristics are based on DE 1 data. Effort was made in doing these calculations to produce results which could be compared with DE 1 RIMS data for the light ions. In addition to velocity distributions, the semikinetic model gives altitude profiles of density, drift speed, parallel and perpendicular temperature and parallel and perpendicular heat flow. Comparisons between density and drift speed from the model are then made with the average of these quantities from the light ion data. Additionally, the skew of the RIMS ion spin curves (counts versus spacecraft spin phase) is used to compare with synthetic spin curves produced from the model velocity distributions.

RIMS ION DATA IN THE POLAR CAP

Among the inputs needed for the semikinetic model are the altitude profiles of the O^+ density and temperature as well as the electron temperature. Figure 1 shows RIMS data for O^+ density versus altitude. The small dots in the figure are individual measurements and the large filled circles are mean values of all measurements in a 500 km interval centered on the large circle. The individual O^+ density values were obtained from RIMS O^+ spin curves by the method outlined in Chandler et al. /2/. These measurements were taken during the declining phase of the solar cycle between December 1981 and December 1983 at invariant latitudes greater than 76°. The decrease in the mean values below 1500 km is due to an instrument safety feature which prevented it from observing densities much larger than 10^4 cm^{-3}. The O^+ densities are reliable above about 1700 km.
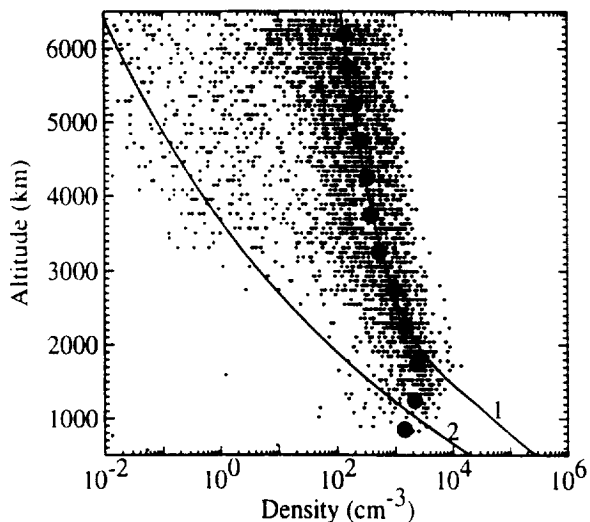

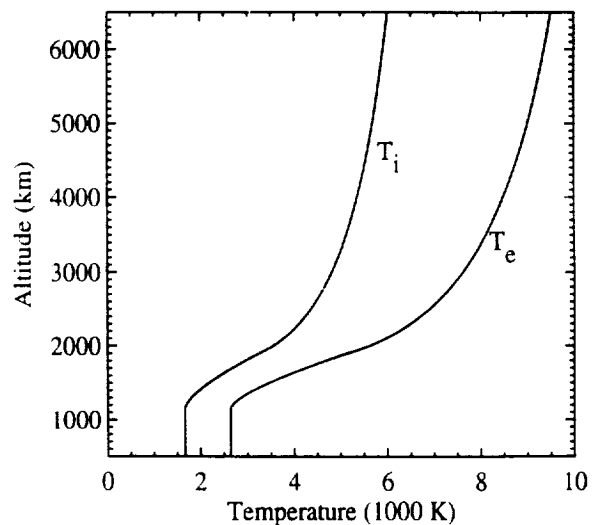Fig. 1. O^+ densities in the polar cap   Fig. 2. Temperature profiles

The two curves (labeled '1' and '2') in figure 1 are solutions to the O^+ continuity and momentum equations assuming quasineutrality with the electrons and a zero O^+ drift speed. For these solutions temperature profiles for the electrons and the O^+ ions were needed. These were obtained assuming a constant temperature at low altitude and then an increasing temperature with altitude which followed a functional form obtained by assuming that the heat flux was constant and proportional to the gradient of the temperature. The constant of proportionality was assumed to be proportional to $T^{5/2}$ according to Spitzer /11/. A temperature profile is then determined by its values at the two end points and specification of the point, r', where it goes from being constant to being heat flow dominated. For the two curves in figure 1 the temperatures at the lower boundary where taken from the IRI-90 model. For curve 1 the conditions assumed were spring time, 830

local time. Ap=18.6 and $F_{10.7}$ = 150 (a large fraction of the data were collected under these conditions). For Curve 2 the conditions assumed were winter time, 830 local time, Ap=18.6 and $F_{10.7}$ = 80. The temperature profiles which correspond to density profile 1 in figure 1 are shown in figure 2. The temperatures at the upper boundary and the point r' where adjusted so that the density profile matched the mean O^+ densities from the data. The sum of the electron and O^+ temperatures at the upper boundary for this case is 15,500 K which is consistent with what is needed to match electron densities at higher altitudes assuming that O^+ is the dominant ion to higher altitudes over the polar cap /12/. For density curve 2 the temperatures were assumed to be constant with altitude. These density and temperature profiles were used as model inputs.

In addition to sampling O^+, the RIMS instrument also made measurements of H^+ and He^+. Figure 3 shows four examples of H^+ spin curves at the altitudes and invariant latitudes indicated. During the same two year period described above, the RIMS instrument collected about 3500 1-minute averaged spin curves (like those in figure 3) for both H^+ and He^+ in the 600 km – 6378 km altitude range and in the 76° – 90° invariant latitude range. Two bulk parameters which can be obtained from these curves are the density and field-aligned flow speed as discussed by Chandler et al. /2/. In addition, the shape of the spin curve carries information about the form of the ion velocity distribution. During the period of data collection the radial head of the RIMS instrument operated as an integral instrument. The spin curve then represents a projection (or shadow) of the three-dimension velocity distribution as seen from the point in velocity space determined by the difference between the spacecraft velocity and the ion bulk velocity. If the velocity distribution is symmetric with respect to the magnetic field direction as well as being gyrotropic its spin curve will be symmetric from any velocity space vantage point. Skewness of the spin curve is an indication of a departure from isotropy in the velocity distribution. Because of the geometry of the orbit of DE 1, a negative skewing of the spin curve indicates that the velocity distribution is skewed, or elongated, in the downward field-aligned direction. Positive skewing indicates the reverse.
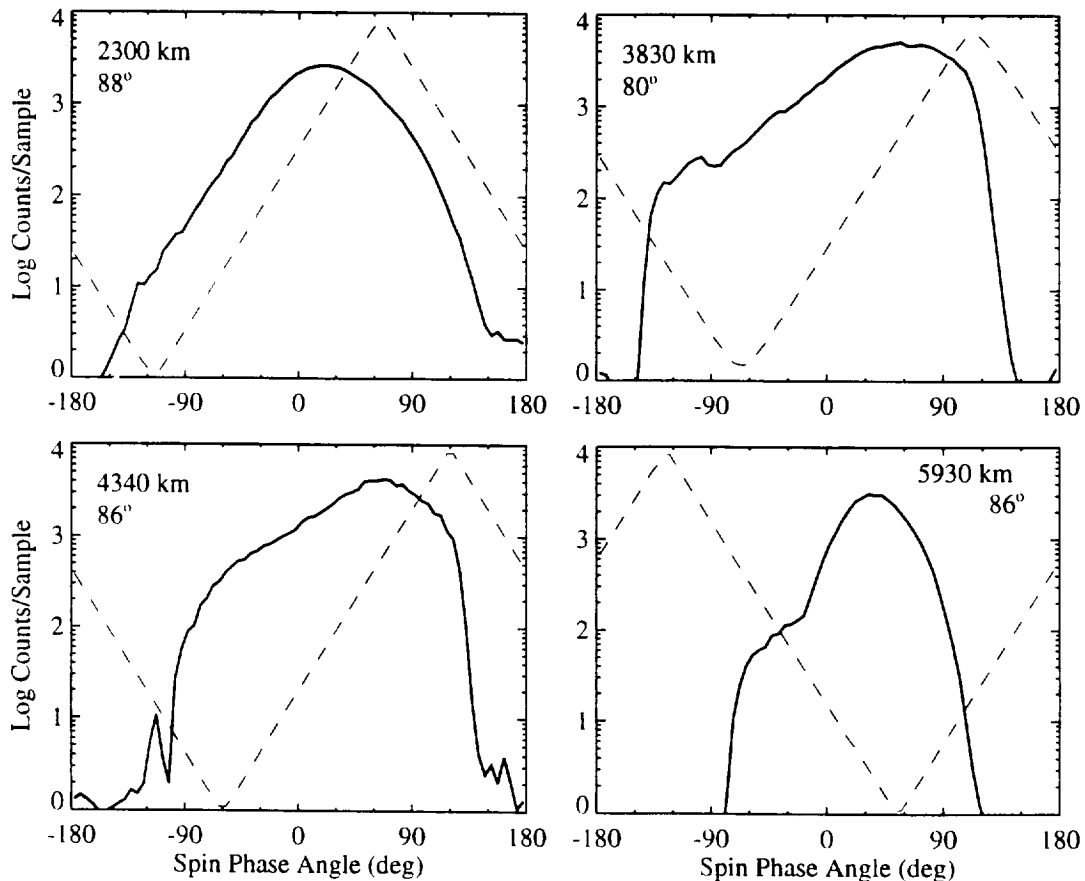

Fig. 3. Sample DE 1 RIMS H^+ spin curves

The semikinetic model used here for the transition region calculations is nearly the same as that presented in Wilson /7/. Both hydrogen and Helium ions, subjected to the ambipolar electric, gravitational and magnetic mirror forces, are followed in their one dimensional motion along a radial field line. Ion velocities are deflected each time step with random velocity impulses whose distribution has a mean of zero and a deviation determined by the local collision frequency /10/. Both of these light ions collide with the dominate O^+ ion and with themselves while H^+–He^+ collisions are ignored. This time-dependent model is run until steady-state is reached and then time averaged to produce the output. The hydrogen ions are created and removed (mostly in the lower portion of the flux tube) by the accidently resonant charge exchange reaction

$$H^+ + O = H + O^+ \tag{1}$$

An additional source of H^+ is the photoioization of atomic hydrogen. For these reactions the model requires altitude profiles of O, H and the neutral temperature (in addition to O^+) which come from the MSIS-86 model /13/. The He^+ ions are created by photoionization of He and removed mainly by reaction with N_2. These reactions require altitude profiles for He and N_2 which also come from the MSIS-86 model.

Figures 4 and 5 show the results for a case (case 1) done using the O^+ density profile from figure 1 (curve 1) and the O^+ and electron temperature profiles from figure 2. The conditions chosen for both the MSIS-86 and IRI-90 models used to generate input for this case were spring time (day 82), local time = 830, Ap = 18.6, 80° magnetic latitude, and $F_{10.7}$ = 150. The four panels in figure 4 show the density of all three ion species, the hydrogen and helium field-aligned drift speeds and the parallel ('z') and perpendicular ('p') temperatures and parallel and perpendicular heat flows of hydrogen and helium (solid line – H^+, dashed line – He^+). The two columns in figure 5 show normalized velocity distribution plots for both H^+ and He^+ at the indicated altitudes. Each curve in the velocity contours is separated by $e^{-1/2}$. Apparent in these results is that O^+ is the dominant ion species at all altitudes, followed by H^+ then He^+. The H^+ drift speed exceeds the He^+ drift speed at all altitudes and both drift speeds are increasing throughout this altitude range. Both light ion species experience primarily perpendicular heating as they collide with the O^+ in the 1000–2500 km altitude range. In this same region both species have velocity distributions distorted in first the upward direction (positive parallel heat flow) and then the downward direction. At higher altitudes (above 2500 km) the H^+ ions develop a significant amount of negative skewing (negative parallel heat flow) as is apparent in the downward suprathermal tail. This is a result of residual H^+ production at high altitude by the charge exchange reaction in equation (1). The ions created at high altitude do not make a significant contribution to the density or drift speed but they make a small contribution to the parallel temperature and a large contribution to the parallel heat flow. They remain at small field-aligned velocities because they are created at altitudes above the region of strong ambipolar electric field acceleration.

Figures 6 and 7 show results for a case (case 2) which uses the second O^+ density profile from figure 1. This case is shown as a counter point to that shown in figures 4 and 5 to indicate the range of variability in the model results. In the density plots one can see that O^+ is no longer the dominant ion at all altitudes and that the H^+ and He^+ densities are nearly the same, especially at high altitudes. The light ion drift speeds do not continuously increase with altitude and are smaller than the previous case. For both H^+ and He^+ one sees the same basic trend of the parallel and perpendicular temperatures at low altitude, but at high altitude the temperature anisotropy reverses with the parallel temperature becoming the larger of the two. The hydrogen velocity distribution again shows the downward suprathermal tail as seen in the previous case but this tail is larger, relative to the core of the distribution. In this case the downward tail is due mainly to photoionization of atomic hydrogen at high altitude. This source is now more important relative to the charge exchange source because of the smaller amount of O^+ present. The helium ions also have a downward tail but in this case the distribution more resembles a Maxwellian core with a shoulder on the downward velocity side. These ions are the result of helium ions created at high altitude which become trapped in a potential well created on the low altitude side by the strong
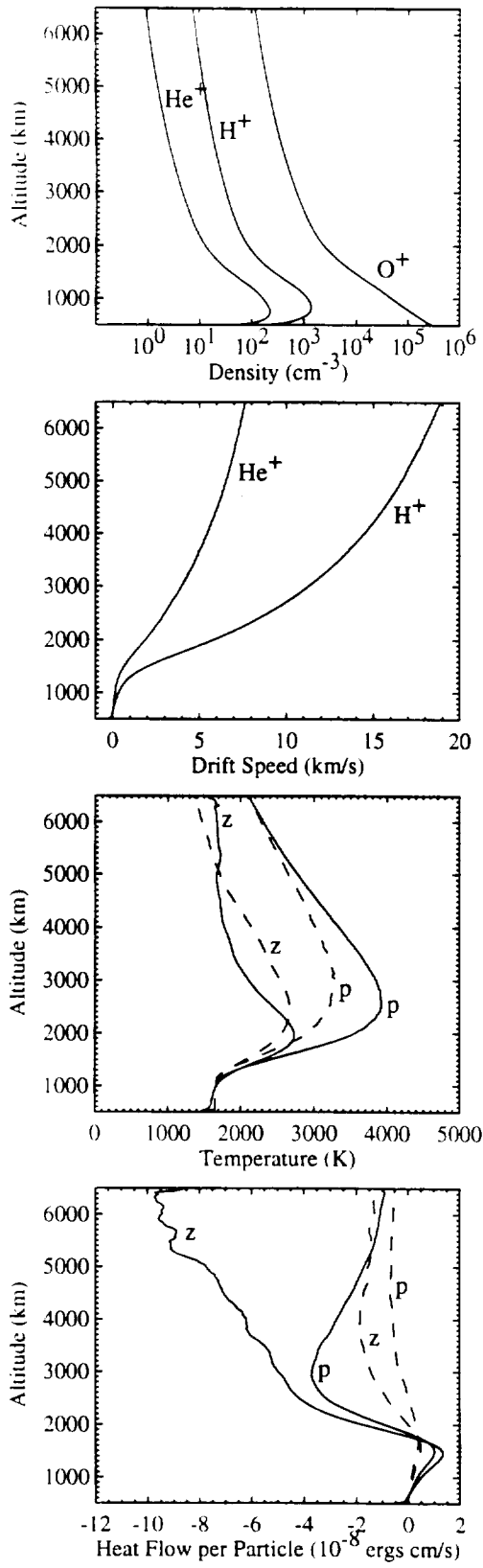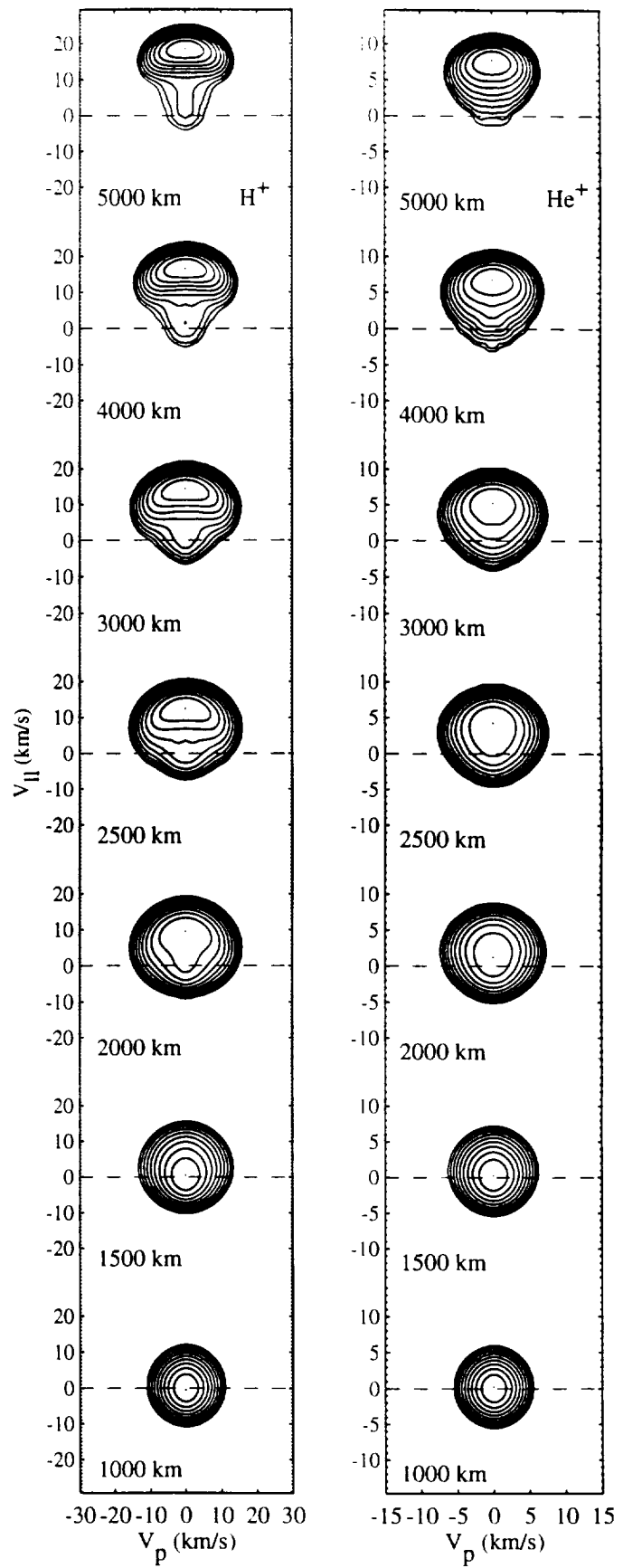
Fig. 4. Bulk parameters for case 1.

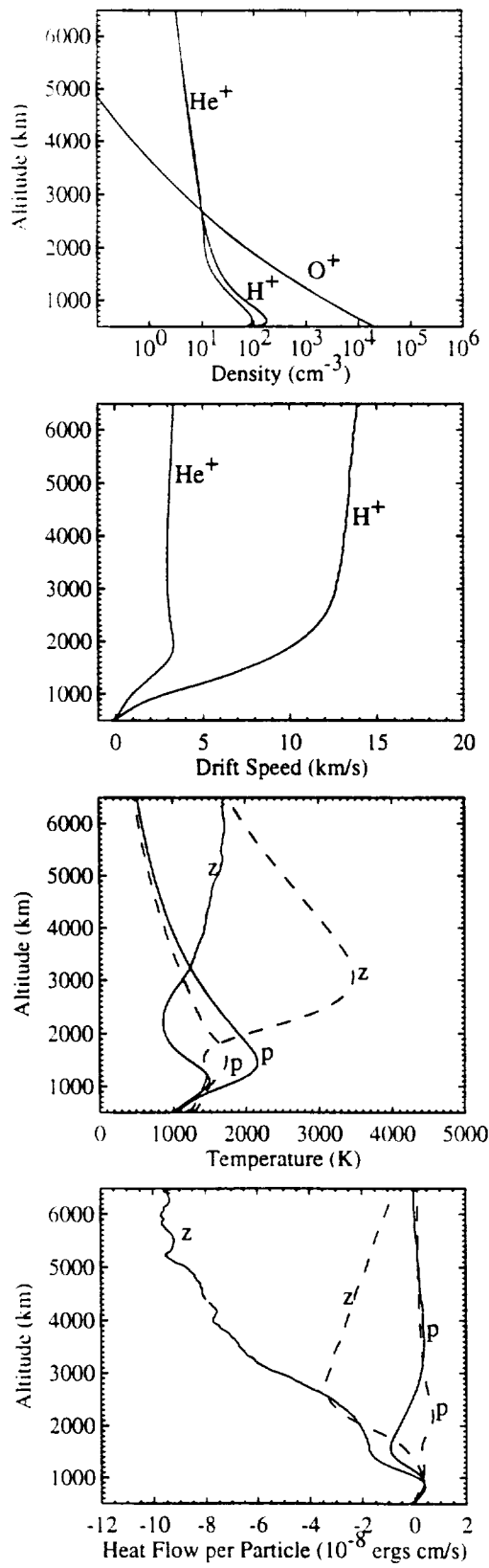Fig. 5. Velocity distributions for case 1.
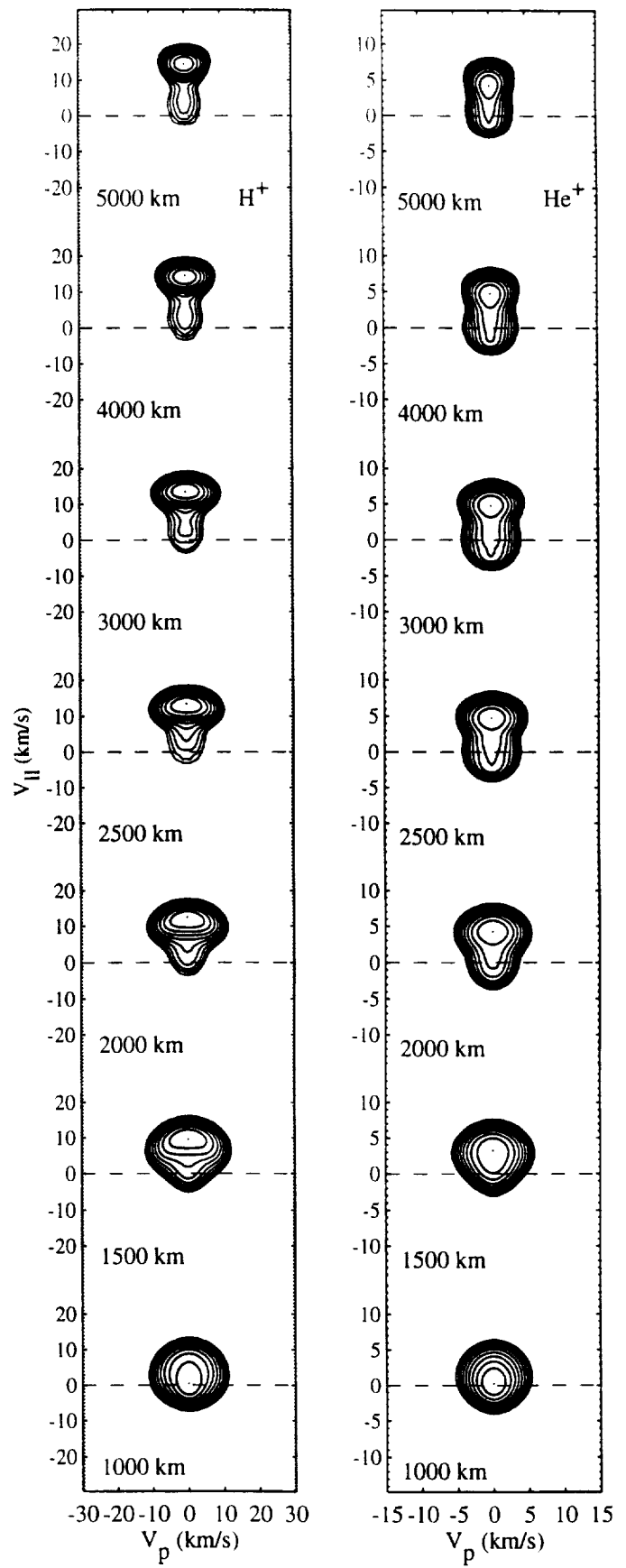
Fig. 6. Bulk parameters for case 2.

Fig. 7. Velocity distributions for case 2.

upward ambipolar electric field (where the electron density gradient is large) and on the topside by gravity. At high altitudes the electric field is not strong enough, because of the small density gradient and the low electron temperatures, to allow the helium ions created there to overcome the gravitational barrier.

COMPARISON OF MODEL RESULTS WITH THE RIMS DATA

Figure 8 compares the density and drift speed profiles from the two cases discussed in the previous section with the mean values of the density and drift speed from the RIMS polar cap data. The large filled circles and diamonds give the mean values for each quantity in a 500 km interval centered on the point. The solid curves labeled '1' are the corresponding quantities from the case shown in figures 4 and 5 while those labeled '2' correspond to figures 6 and 7. It should be emphasized here that unlike the case with the O^+ density in figure 1, there is more scatter of the data around the mean values than is present there. These ion data were collected under a wide range of solar and geomagnetic conditions during the course of two complete seasonal cycles. Never the less, there does appear to be consistent trends in the mean data and there is good agreement, at least at low altitude, with the results of case 1. The most important discrepancy between the mean data and the model results is the disagreement between the H^+ drift speeds at altitudes above 3000 km. A number of other cases were done with different input parameters and in each case the model drift speeds were well above the mean of the data. On average, about 90% of the measured H^+ drift speeds lie well below the model drift speeds above 3000 km.
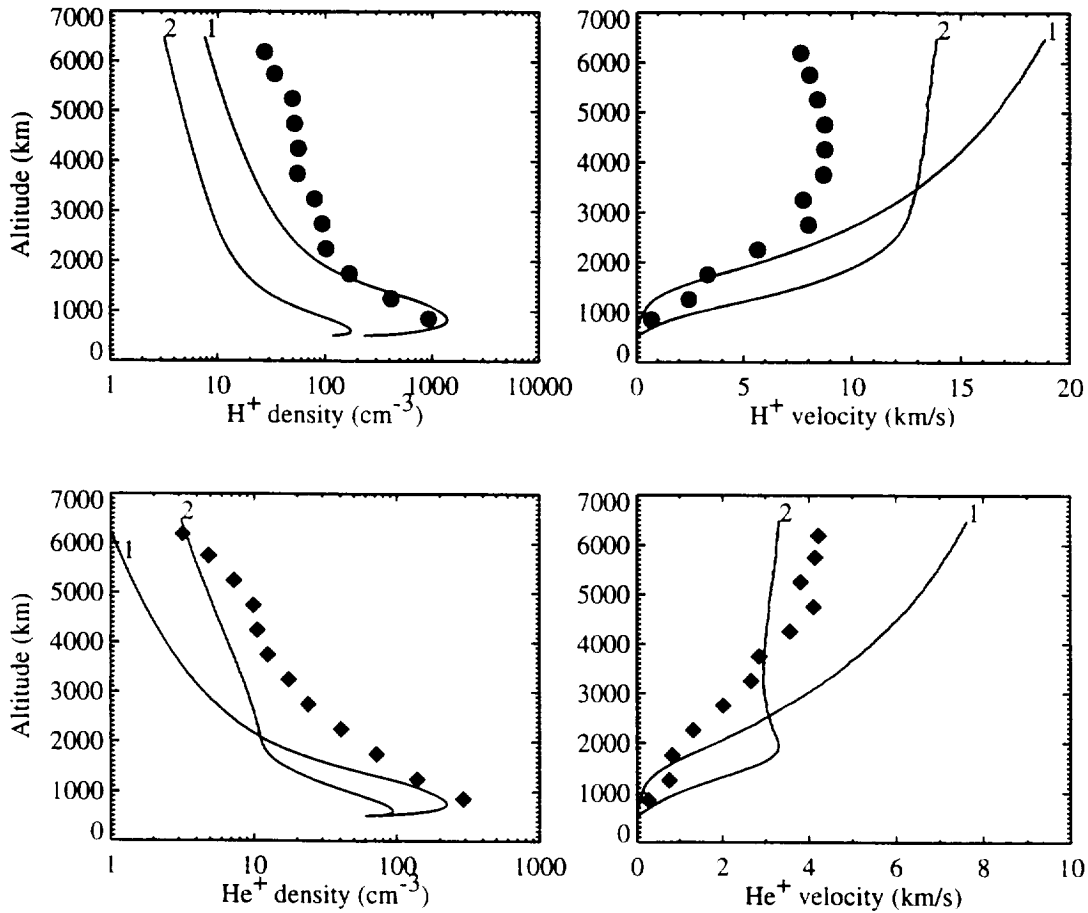
Fig. 8. Comparisons between model results and mean data values.

Another point of comparison between the data and the model results can be made by comparing the shape of the spin curves. To do so we took a model designed to simulate the response of the RIMS instrument and adapted it to take as input the model velocity distributions. As additional inputs the model requires, the spacecraft velocity in a coordinate system fixed to and aligned with the local magnetic field, and the spacecraft potential. The spacecraft velocity is largely constrained

by the geometry of the orbit of DE 1 in the polar cap region. Because apogee was well above 1 Re altitude the spacecraft was either ascending or descending when it was at altitudes less then 1 Re over the polar cap. The spacecraft potential is unknown but estimates based on the densities and temperatures from the model suggest that it would range from about -1 V at 600 km to about 2 V at 1 Re. As an example, figure 9 shows synthetic spin curves for the H$^+$ velocity distribution at 4000 km from figure 5. The top row of plots are for an ascending space craft trajectory while the bottom row are for a descending trajectory. The range of assumed spacecraft potentials is indicated in each plot. One can see that the downward skewing of the velocity distribution is more apparent for an ascending trajectory with a small spacecraft potential. Figure 10 shows an ascending trajectory, zero potential spin curve for the H$^+$ velocity distribution at 4000 km in figure 7. More skewing of the spin curve is apparent here because of the large suprathermal tail. Some of the spin curves from these two figures resemble the fourth spin curve in figure 3.
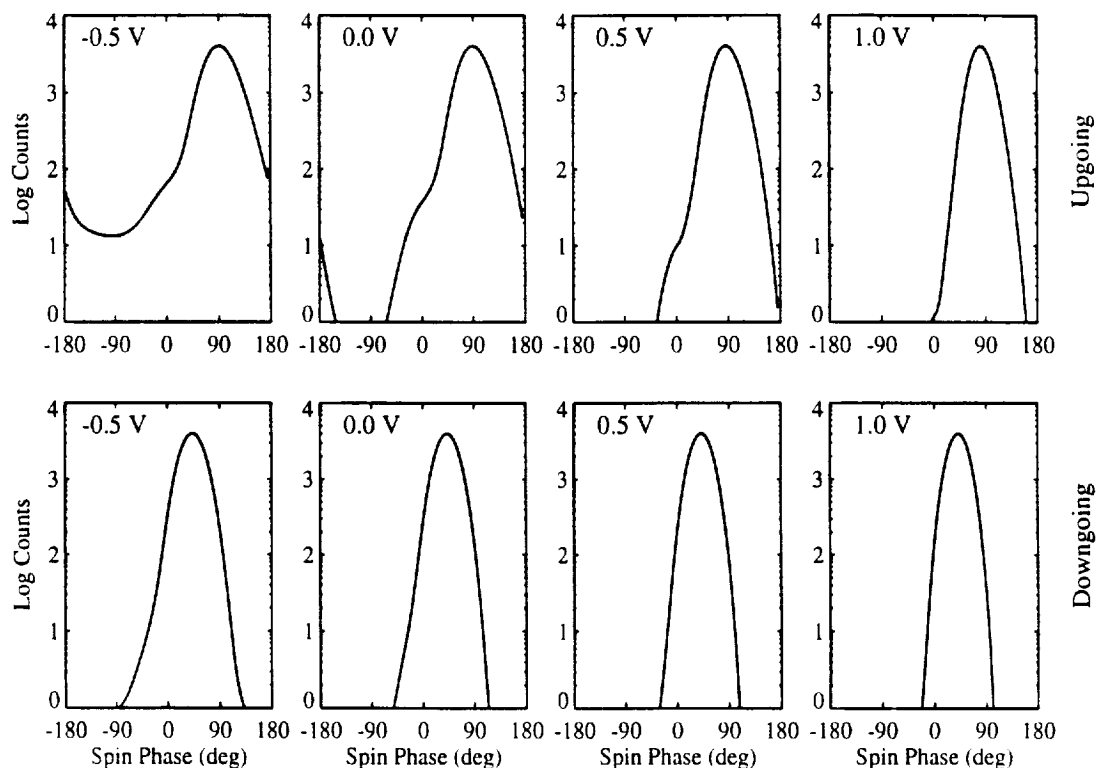

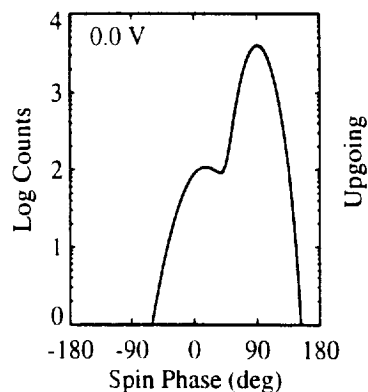Fig. 9. Spin curves for H$^+$ in case 1 at 4000 km.

Fig. 10. Spin curve from case 2.

Although it is possible to produce spin curves from the model velocity distributions which resemble some of the spin curves in the data, many of the observed spin curves have much more skewing than can be accounted for by the model results present thus far. What is needed are velocity distributions which are much broader with more extended downward tails or shoulders than are seen in the velocity distributions in figures 5 or 7. Figure 11 shows two H$^+$ velocity distributions

at 4000 km for a case where a downward flux of H^+ ions was assumed at the upper boundary and a case where an electric potential jump of 1.4 V was assumed at the upper boundary. As can be seen, both distributions have more extensive downward tails then in the previous results. Figures 12 and 13 give the corresponding spin curves for these two distributions in the same format as figure 10. These type of distributions can produce spin curves that resemble some of the more common types seen in the data such as the second and third curves in figure 3. The presence of a high altitude source of downward H^+ flux or a potential barrier has the added benefit of reducing the H^+ drift speeds at higher altitudes (above 3000 km) while leaving the lower altitude velocities unchanged. It can also raise the H^+ density in the model so that it more closely agrees with the mean densities.
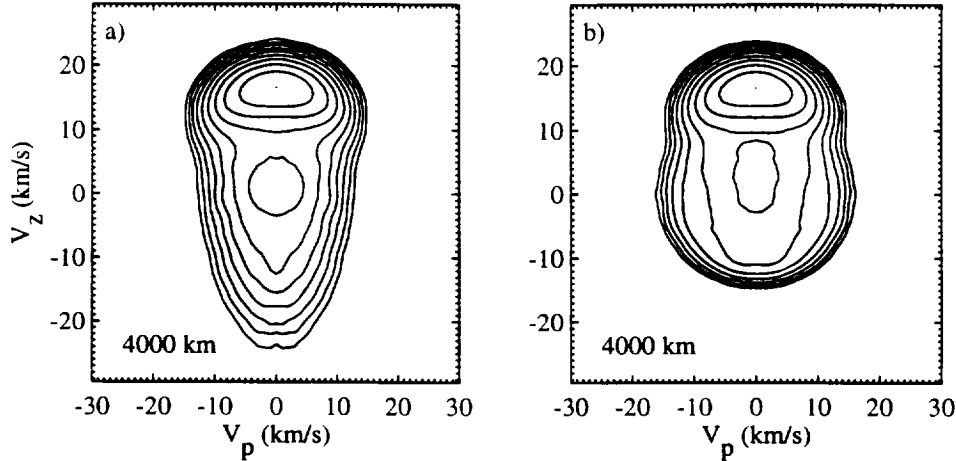

Fig. 11. H^+ velocity distributions for a) downward flux and b) 1.4 V potential barrier.
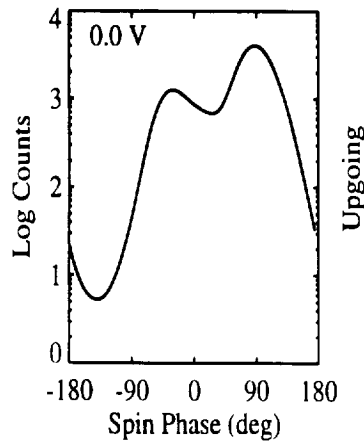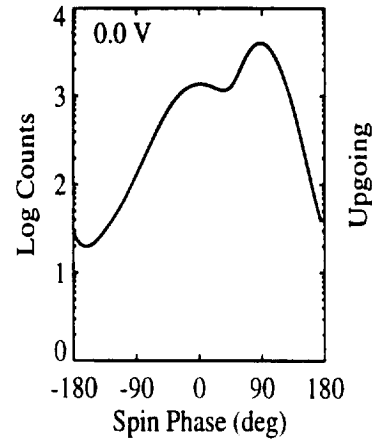

Fig. 12. Spin curve for 11 a).   Fig. 13. Spin curve for 11 b).

At present these results only suggest the presence of downflowing H^+ or potential barriers over the polar cap. An additional mechanisms which might explain the large spin curve skews is the drag on the outflowing H^+ ions that would result from waves driven unstable by the relative streaming of the H^+ and O^+ ions. However, analysis of the model results using the Penrose criterion shows that these distributions are stable against the growth of ion acoustic waves. Analysis of their stability to the growth of ion cyclotron waves has not yet been done. It has also been suggested that time-dependent convection processes may produce results like those seen in figure 11. The semikinetic model is time-dependent so that convection or other time-dependent processes could be studied. Such tasks will be pursued in the near future. In an effort to better understand what the large spin curve skews mean we are currently doing statistical studies of the data to see how the spin curve skews relate to location in the polar cap region or to geophysical conditions.

CONCLUSIONS

Results from the semikinetic model presented in this paper show that under realistic steady-state conditions, the velocity distributions of the H^+ and He^+ ions flowing out of the ionosphere in the

polar cap can deviate significantly from Maxwellian. Often they develop downward skewing in the form of a downward suprathermal tail or shoulder on the core distribution. This results in part because of the collisional drag these ions experience as they flow upward through the nearly static O^+ ions and because of small amounts of residual ion production at altitudes above where most of the polar wind acceleration occurs. Because of the resemblance between the spin curves produced from such model distributions and those seen in the data we believe that such nonMaxwellian velocity distributions exist in this region and are explained by the model. However, we have seen many spin curves which are more skewed than those produced by the simple model. These larger skews indicated that the velocity distributions are more anisotropic than the model indicates. To try to produce such distributions and corresponding spin curves, we tried various processes including a downward flux of ions at the top boundary and a potential jump at the top boundary. These two effects were able to give spin curves which resemble more closely those common in the data. Although these two processes are strong candidates for explaining the spin curves with large skews, much more work is needed to firmly establish this.

REFERENCES

1. R. W. Schunk, The polar wind, in: *Modeling Magnetospheric Plasma*, eds. T. E. Moore and J. H. Waite. Jr., AGU Geophys. Monogr. Ser. vol. 44, Washington, DC 1988, p. 219.

2. M. O. Chandler. J. H. Waite. Jr. and T. E. Moore. Observations of polar ion outflows, *J. Geophys. Res.* 96. 1421 (1991).

3. J. Lemaire. O^+, H^+ and He^+ ion distributions in a new polar wind model, *J. Atmos. Terr. Phys.*, 34. 1647 (1972).

4. H. G. Mitchell, Jr., and P. J. Palmadesso, A dynamic model for the auroral field line plasma in the presence of field-aligned currents, *J. Geophys. Res.*, 88, 2131 (1983).

5. S. B. Ganguli. H. G. Mitchell, Jr., and P. J. Palmadesso, Behavior of ionized plasma in the high latitude topside ionosphere: The polar wind, *Planet. Space Sci.*, 35, 703 (1987).

6. Á. Körösmezey, C. E. Rasmussen, T. I. Gombosi and G. V. Khazanov, Anisotropic ion heating and parallel O^+ acceleration in regions of rapid $E \times B$ convection, *Geophys. Res. Lett.*, 19, 2289 (1992).

7. G. R. Wilson. Semikinetic modeling of the outflow of ionospheric plasma through the topside collisional to collisionless transition region, *J. Geophys. Res.*, 97. 10,551 (1992).

8. I. A. Barghouti. A. R. Barakat and R. W. Schunk, Monte Carlo study of the transition region in the polar wind: An improved collision model. *J. Geophys. Res.*, 98, 17,583 (1993).

9. A. R. Barakat and J. Lemaire, Monte Carlo study of the escape of a minor species. *Phys. Rev. A*, 42. 3291 (1990).

10. T. Takizuka and H. Abe, A binary collision model for plasma simulation with a particle code, *J. Comput. Phys.*, 25. 205 (1977).

11. S. Spitzer. *The Physics of Fully Ionized Gases*, Interscience, New York. 1956.

12. C. W. Ho and J. L. Horwitz, Warm O^+ polar wind and the DE-1 polar cap electron temperature profile. *Geophys. Res. Lett.*, 20, 1751 (1993).

13. A. E.. Hedin. MSIS-86 thermospheric model. *J. Geophys. Res.*, 92. 4649 (1987).

Kinetic modeling of O⁺ upflows resulting from E×B convection heating in the high-latitude F region ionosphere

G. R. Wilson

Department of Physics and Center for Space Plasma and Aeronomic Research, University of Alabama, Huntsville

Abstract. We report here the results of modeling work aimed at understanding the development of ionospheric O⁺ field-aligned upflows that develop in response to high-latitude **E**×**B** drift induced frictional heating. The model used is a collisional semikinetic model which includes ion-neutral resonant charge exchange and polarization collisions as well as Coulomb self-collisions. It also includes the process of chemical removal of O⁺ as well as all of the macroscopic forces: ambipolar electric, gravity, magnetic mirror, and centripetal. Model results show the development of several types of non-Maxwellian velocity distributions including toroids at low altitude, distributions with large heat flow in the perpendicular component at intermediate altitudes, and distributions with a separate upflowing population or upward superthermal tail at high altitudes. Whenever the convection electric field increases from a small value (< 25 mV/m) to a large value (100–200 mV/m) in 6 min or less large upflows develop with parallel drift speeds which peak (below 1000 km) at values between 500 m/s and 2 km/s, parallel fluxes which peak between 6.0×10^8 and 3.2×10^9 cm^{-2} s^{-1}, and parallel per particle heat flows which peak between 8.0×10^{-9} and 8.0×10^{-8} ergs cm/s. The higher values in these ranges occur for a cooler neutral atmosphere, with a larger convection electric field that is turned on quickly. The model produces field-aligned O⁺ flow speeds that are larger than those produced by a 20-moment generalized transport model but smaller then those produced by an isotropic hydrodynamic model for comparable values of the convection electric field and convection turn on times. The model results compare favorably with some topside satellite and radar data.

1. Introduction

The convection path and speed of plasma in the high-latitude ionosphere is highly dependent on processes occurring in the magnetosphere and the solar wind. Unlike the ionosphere at low latitudes that generally corotates with the Earth, the high-latitude ionosphere can follow complex trajectories at highly variable speeds. The convection electric field which drives this plasma flow via the **E**×**B** drift can have values as large as 250 mV/m which gives a convection speed of about 5 km/s in the lower F region. This process, along with thermospheric winds, can lead to a situation where the ions and neutrals flow at large speeds relative to each other in a direction perpen-

dicular to the magnetic field. Since ion and neutral thermal velocities in the lower F region are typically less than 1 km/s, it is possible, during episodes of enhanced convection electric fields, for the ion-neutral relative flow to be supersonic. When this happens significant perpendicular ion heating can occur as the ions and neutrals collide. As has been known for some time, with a large enough **E**×**B** drift, resonant charge exchange collisions between O and O⁺ can produce toroidal ion velocity distributions [*Schunk and Walker*, 1972; *St-Maurice and Schunk*, 1979; *Barakat et al.*, 1983; *Winkler et al.*, 1992].

Frictional heating of O⁺ ions at low altitude will lead to enhanced O⁺ upflows. This mechanism can explain at least some of the upflows which are seen by radar [*Yeh and Foster*, 1990; *Keating et al.*, 1990; *Wahlund et al.*, 1992] and low-altitude satellites [*Tsunoda et al.*, 1989; *Loranc et al.*, 1991; *Anderson et al.*, 1991]. These data sets provide a great deal of information concerning the chief characteristics of these upflows,

what they are associated with and where they occur. Upward velocities in these events (at altitudes of 1000 km or less) are typically around a few hundred meters per second although values above 1 km/s are not uncommon and as high as 3 km/s values have been seen. Generally, the velocities increase with altitude. Fluxes in these enhanced upflow events range from 10^8 to 10^{10} cm^{-2} s^{-1} with typical values near 10^9 cm^{-2} s^{-1} or a few times 10^9 cm^{-2} s^{-1}. Sometimes, but not always, the ion temperature is elevated in these events. Typical elevated values range from 1500 K to about 10,000 K. There is also evidence, in some events, for temperature anisotropy at low altitude with $T_\perp > T_\parallel$. In some events the electron temperature is elevated, and in some it is not. In some events the bottomside electron densities are increased, while in others they are reduced. These upflows are seen most often in the auroral zone, the cusp region and the subauroral region on the nightside in so-called "SAID" (subauroral ion drifts) events. They are associated with regions of field-aligned current, enhanced convection electric fields, convection shears, and regions of energetic ion and/or electron precipitation.

There are other possible mechanisms, besides frictional heating, which could account for these upflows. These include current-driven wave heating [*Providakes and Seyler*, 1990], energetic electron precipitation (giving elevated electron temperatures and ambipolar electric fields [*Barakat and Schunk*, 1983]), ionization of energetic neutral oxygen backsplash that results from ring current ion precipitation [*Torr and Torr*, 1979; *Kozyra et al.*, 1982], the auroral density cavity "vacuum cleaner" effect [*Singh et al.*, 1989], and joule heating and subsequent expansion of the neutral atmosphere [*Millward et al.*, 1993]. In many situations, no doubt, several of these processes act in concert to produce the net effect. In order to determine how much of the observed upflow is a result of frictional heating or when an upflow event is dominated by frictional heating, it is necessary to study this process alone to determine its maximum effect and the characteristics of the generated upflow.

The central question in this paper is: How much O$^+$ upflow will result from $\mathbf{E} \times \mathbf{B}$ driven frictional heating in the F region ionosphere and what characteristics will this outflow have (i.e., fluxes, drift speeds, temperatures and heat flows, velocity distribution characteristics, etc.)? The answer to this question will depend on the interplay of a variety of processes including ion-neutral collisions, ion-neutral reactions, ion self-collisions and the various macroscopic forces such as gravity, the mirror force, the ambipolar electric force, and the centrifugal force. The collision and reaction processes are highly dependent on ion energy, and as such, their overall effect will be sensitive to the type of ion velocity distribution present. The effect of the mirror force is also dependent on the ion velocity distribution. In addition to the reactions, collisions, and forces, the time history of the frictional heating event will also play a role.

In the last few years there have been a number of studies of the F region plasma flows that develop in response to low-altitude frictional heating. Most of these studies have used various types of hydrodynamic or generalized transport models. *Gombosi and Killeen* [1987] used a hydrodynamic model, which included most of the low-altitude chemical and collisional processes, to study the effect of a short-duration (about 5 min) low-altitude frictional heating event. In this event the peak, column-integrated heating rate was 100 ergs cm^{-2} s^{-1}. In response, an O$^+$ upflow, with a flux of about 10^8 cm^{-2} s^{-1} (normalized to 1000 km) developed. Above 5000 km the O$^+$ flow speed approached 2 km/s. *Cannata et al.* [1988], using the same model, studied the response of a convecting flux tube following realistic convection paths and subject to neutral winds derived from the thermospheric global circulation model (TGCM) to estimate the heating rates used. They concluded that such heating can perturb the ionosphere and that gradients in the heating rate may be more important than the absolute heating rate in determining the amount of upflow which develops.

In a series of papers [*Sellek et al.*, 1991; *Moffett et al.*, 1991; *Heelis et al.*, 1993] an isotropic hydrodynamic model for a closed $L = 4$ flux tube is used to examine the ionospheric response to SAID events for different neutral atmospheres (variation in $F_{10.7}$) and for various ramp times for the turn on of convection. In each case the convection speed was increased linearly from 0 to 2 km/s in periods of time ranging from 15 s to 10 min. Results of these studies show the O$^+$ temperature increasing from a value near 1200 K to values of 3200 to 4500 K at 300 km altitude. Below 400 km field-aligned flows are downward but above 500 km upward flows develop and reach speeds as high as 1.9 km/s when the convection speed is turned on rapidly. O$^+$ fluxes at 1000 km altitude range from values of about 2×10^8 to about 5×10^9 cm^{-2} s^{-1} with increasing $F_{10.7}$. The maximum O$^+$ field-aligned drift speed also increases from solar minimum to solar maximum.

Körösmezey et al. [1992] used a more sophisticated 20-moment generalized transport model to follow a flux tube through a 3 km/s SAID event. They showed that significant ion temperature anisotropy develops in the low-altitude region and that a wave like pulse of velocity travels up the flux tube even during a period of constant heating. Below 1000 km the O$^+$ parallel drift velocity never exceeded +300 m/s for this case. When the convection drift speed was increased to 4 km/s, the maximum parallel drift (below 1000 km) reached +400 m/s. One possible reason for the relatively low parallel drift speeds (compared to the isotropic hydrodynamic results) may be the allowance for temperature anisotropy in the 20-moment model which would lead to a smaller parallel temperature increase and a reduction in the pressure gradient force. However, the parallel temperature at 200 km does reach a value as high or higher then is seen in the hydrodynamic results for a convection speed of 3 km/s.

The work of *Loranc and St-Maurice* [1993] addresses the study of low-altitude frictional heating from a significantly different perspective. They used a collisionless kinetic model to study the type of outflows which

develop above the exobase (taken at 500 km). To simulate a frictional heating event, they increased the ion temperature at the lower boundary from 1000 to 5000 K in a period of from 2 to 50 s, held the temperature constant for a few minutes and then returned it to the lower value. The results of this work showed very large parallel drift velocities, between 2 and 3 km/s (below 1000 km altitude), with upward fluxes exceeding 10^9 cm^{-2} s^{-1}. Frequently, non-Maxwellian velocity distributions with two distinct ion populations were produced.

In comparing the isotropic hydrodynamic model, the 20-moment generalized transport model and the collisionless kinetic model, it is apparent that large differences in the results (field-aligned flow speed) can be found depending on whether the model has isotropic or anisotropic temperatures, is collisional or collisionless or includes kinetic processes (free streaming, multiple populations and velocity dispersion). What is needed is a model which allows for anisotropic temperatures and includes both collisions and kinetic processes. Such a model will allow the determination of the effect of these various processes on the outflows which develop. In this paper we present the results of a study of F region $\mathbf{E} \times \mathbf{B}$ frictional heating using a collisional kinetic model which includes all of these processes. Details of the model are described in the next section, with results in the section following.

2. Description of the Model

The model used for this work was derived from a semikinetic, time-dependent, plasma transport model originally developed for the study of the outflow of ionospheric plasma at polar latitudes [*Wilson et al.*, 1990] and modified to study the collisional to collisionless transition region [*Wilson, 1992*]. In this study the model was further modified to include ion-neutral collisions and reactions. Only the O$^+$ ion is followed, in a simulation region extending from 300 km to 1100 km. The semikinetic model differs from hydrodynamic or generalized transport models in that the ions are described through the behavior of a large number of simulation particles rather than with a set of velocity moments and transport equations. We do not follow the full ion cyclotron motion of the simulation ions but instead follow the motion of their gyrocenters. This approximation is valid if the gyroperiod is small compared to any other timescale in the problem. This condition is satisfied by all of the results presented in this paper. As the simulation gyrocenters move along the magnetic field line (assumed vertical), they are acted on in a continuous fashion by several large-scale macroscopic forces and in a random fashion by various microscopic collision and reaction processes.

The total field-aligned, macroscopic force acting on a singly charged O$^+$ simulation ion is given by

$$F_\parallel = m\frac{dv_\parallel}{dt} = eE_\parallel + mg_\parallel + \mu\nabla_\parallel B + 1.5\frac{r^2}{r_0^3}\frac{E_c^2}{B_0^2} \quad (1)$$

In (1), $E_\parallel$ is the ambipolar electric field along the magnetic field direction, $g_\parallel$ is the component of $\mathbf{g}$ along $\mathbf{B}$. E_c is the magnitude of the perpendicular,

convection electric field at the lower boundary (r_0), and B_0 is the intensity of the magnetic field at r_0. The rest of the symbols in (1) have their usual meaning (i.e., t, time, m, ion mass, μ, magnetic moment, $\nabla_\parallel$, spatial gradient along the magnetic field; etc.) The ambipolar electric field is found by differentiating the ambipolar electric potential. The potential is found by assuming quasineutrality between the ions and electrons and assuming the electrons are isothermal and Boltzmann distributed. With this approach and an assumed value of the electron temperature ($T_e = 2000$ K), knowledge of the ion density is all that is needed to find $E_\parallel$ since

$$n(O^+) = n_e = n_{eo}\exp\left(\frac{-e\Phi_E}{kT_e}\right) \quad (2)$$

We use a value of 2000 K for the uniform electron temperature since we wish to concentrate on the effect of ion frictional heating on ion upflows. Of the four forces listed in (1) the smallest contribution is made by the centrifugal force, at least over the altitude range considered here.

The O$^+$ ion will undergo a number of different types of ion-neutral collisions. With neutral species other than atomic oxygen the collision is primarily the polarization collision where the ion interacts with the electric dipole that it induces in the neutral. With atomic oxygen O$^+$ ions will experience both polarization and resonant charge exchange (RCE) collisions. It is the O$^+$-O RCE collisions that are primarily responsible for the formation of toroidal velocity distributions. For O$^+$-O collisions the cross section is dominated by polarization collisions at low energies ($T_r < 400$ K for colliding Maxwellians) and by RCE collisions at high energies [*Knof et al.*, 1964; *Banks and Kockarts*, 1973].

The method used to treat O$^+$-O collisions is essentially that used by *Barakat et al.* [1983]. During each time step, for each simulation ion, a random neutral oxygen velocity is generated from a nondrifting Maxwellian velocity distribution with the neutral exospheric temperature. When E_c is nonzero, an additional velocity component is added to the neutral's velocity to account for the relative convection drift between ions and neutrals. (Strictly speaking this drift velocity should be added to the ion's velocity but because of the interchangability of reference frames the collision calculations proceed identically regardless of where the drift velocity is added.) The relative speed g between the ion and this neutral is then found. With this speed and the atomic oxygen density, a random impact parameter b is generated based on Poisson statistics

$$b = \sqrt{-\frac{\ln(1-r)}{\pi n(O)gdt}} \quad (3)$$

where dt is the time step and r is a random number uniformly distributed between 0 and 1. With this same value of g, impact parameters for the polarization and the RCE collision (b_p and b_r) can be found, knowing their respective cross sections [*Barakat et al.*, 1983] and the atomic oxygen density. If $b \leq b_p$ and $b > b_r$

only a polarization collision occurs and the resultant change in the ion's velocity is calculated assuming the collision is elastic and that the ion-neutral relative velocity is deflected through a random angle uniformly distributed between 0 and π. If $b \leq b_r$ and $b > b_p$ an RCE collision occurs, but with a probability of $\frac{1}{2}$. In that case the ion and neutral velocities are switched. If conditions are such that both collisions occur, then both are performed with the order randomly selected so that the RCE collision occurs first half of the time. This collision algorithm was tested by performing local calculations identical to the cases considered in *Barakat et al.* [1983]. Our results agreed with theirs to within 1%.

The above approach to O+–O RCE collisions is an approximate method. The completely rigorous approach to performing these collisions in a particle code would be to find, based on the O velocity distribution and the given O+ velocity, the distribution of the magnitudes of the relative velocity g (i.e. $f(g)$) and then calculate the overall probability of collision during a time step dt by

$$P = 1 - \exp\left(- dtn(O) \int g\sigma_r(g)f(g)dg \right) \quad (4)$$

We assume that $f(g)$ is normalized so that $\int f(g)dg = 1$. If a collision occurs than an O velocity should be randomly selected based on the collision probability of the resulting g value and the O+ velocity would be changed accordingly. Instead of doing this the approach used in the model replaces the integral in the exponential in (4) with $g\sigma_r(g)n(O)dt$ where g is found at each time step as discussed above. There remains the question of how good or bad this approximation is.

If the velocity of the O+ simulation particle is well outside of the region of velocity space where the O velocity distribution dominates, then g will be large and variations in g that result from selecting different O velocities will be small. The approximation of neglecting the integral in (4) is a good one since g is nearly constant. This situation occurs frequently due to the $\mathbf{E} \times \mathbf{B}$ relative drift between the ions and neutrals. Even when the ions develop a toroidal velocity distribution most of the ions are in a portion of velocity space outside of that occupied by the neutrals. When the O+ velocity falls within the velocity space region occupied by the neutrals g and the calculated collision probability will vary widely. However, because particles take many time steps to cross a cell the total probability for collision for this number of time steps will closely approach the correct value since the variability in the probabilities calculated at each time step will average out upon summation.

The only other ion-neutral collision considered is the polarization collision between O+ and N$_2$. The procedure employed is identical to that used for the polarization collisions between O+ and O with the appropriate change in the polarizability constant found in the cross section. Polarization collisions between O+ and other neutrals (O$_2$, N, H, etc.) were not considered since their combined densities where less

than the combined O and N$_2$ density by at least an order of magnitude for all situations that we considered. In order for the ion-neutral collisions to be treated properly the time step must be small enough so that the fraction of simulation ions experiencing one or more collisions in a time step is small. The time step used (0.05 s) was small enough so that at 300 km, for the cases using the solar maximum atmosphere and when the O+ temperature was highest, < 10% of the ions experience one or more collisions in a time step. A few tests, performed using half this time step (0.025 s), showed no significant differences demonstrating that the original time step of 0.05 s is indeed small enough. No effort was made to follow multiple ion-neutral collisions during a single time step since this happens for only a very few particles. For the extreme situation just mentioned Poisson statistics have 9.7% of the particles experiencing only one collision while 0.3% experience two or more.

In addition to collision processes that can energize O+ ions when large ion-neutral relative drifts occur, O+ will be lost via reactions with N$_2$ and O$_2$

$$\begin{aligned} O^+ + N_2 &\rightarrow NO^+ + N \\ O^+ + O_2 &\rightarrow O_2^+ + O \end{aligned} \quad (5)$$
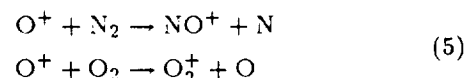
During episodes of frictional heating these reactions can lead to a substantial change in the F region ionosphere [*Schunk et al.*, 1975] since the cross sections for these reactions are known to be highly dependent on the ion-neutral relative energy [*Albritton et al.*, 1977]. In the model we descritized these cross sections and used them to determine whether or not a simulation ion was lost during a time step. The procedure was to generate a random neutral velocity (for either N$_2$ or O$_2$) so that the ion-neutral relative speed g could be found. (This neutral velocity also has the $\mathbf{E} \times \mathbf{B}$ convection component added.) This speed is used to find the appropriate value of the cross section which is used to find the probability of reaction during a time step. Using Poisson statistics and a random number r a decision is made about whether or not a reaction occurs. If it does, the simulation ion is removed. This procedure was tested and found to be working properly since the reaction rate as a function of temperature for reacting Maxwellians was found to agree with rate equations given by *Schunk and Nagy* [1980]. The effect of the ions generated by these reactions was not included in the model. These ions will influence the O+ ions near the lower boundary by changing the ambipolar electric field and by through Coulomb collisions. Both of these effects are expected to be small compared O+–neutral collisions. The accidentally resonant charge exchange reaction with H (another O+ loss process) was also included in the model and handled in the same fashion as the reactions with N$_2$ and O$_2$.

The effects of small angle Coulomb self-collisions are included in the model by use of the method of *Takizuka and Abe* [1977]. If the ion time step is small compared to any of the collisional relaxation times, this method is equivalent to a solution of the Landau form of the Fokker-Planck equation. The small time steps needed for the ion-neutral collisions discussed

above are adequately small for this purpose. For O$^+$–O$^+$ self-collisions the procedure is to randomly pair O$^+$ simulation ions located in the same spatial cell and to compute the deflection of their relative velocity $\vec{U}$ according to that which would result from the cumulative effect of many small angle collisions experienced over the course of a time step. The variable $\delta = \tan(\Theta/2)$ (Θ is the angular deflection of $\vec{U}$) is chosen randomly from a Gaussian distribution with zero mean and a variance $\langle \delta^2 \rangle$ given by

$$\langle \delta^2 \rangle = \frac{e^4 n \ln \Lambda}{2\pi\epsilon_0 m^2 |\vec{U}|^3} dt \qquad (6)$$

where n is the O$^+$ density in the cell, Λ is the plasma parameter, and m is the oxygen ion mass. The resulting change in the relative velocity $\vec{U}$ is applied to both particles so that between them, momentum and energy is conserved. Since these quantities are conserved between each colliding pair, they are conserved for the entire population. Tests of this procedure show that it conserves energy and momentum globally as well as relaxing all velocity distributions to the Maxwellian over the appropriate timescales. In addition, this procedure produces, on average, stopping, deflection and energy exchange frequencies as functions of ion velocity, appropriate for the Coulomb collision.

All of the cases that will be discussed in this paper were done for dayside (1200 LT) conditions. Since the flux tubes were in sunlight, photoionization of O occurs throughout each simulation run. This effect is included through the introduction of simulation ions in each cell at a rate determined by the local atomic oxygen density and the ionization rate determined by solar conditions (1.7×10^{-7} s^{-1} for solar minimum and 4.6×10^{-7} s^{-1} for solar maximum). When new photoions are introduced, they are given a randomly generated velocity drawn from a Maxwellian distribution that is at rest with respect to the neutrals. During the course

of each run this process only had a small effect since each run typically lasted only a few minutes.

As inputs to the model, a neutral atmosphere with altitude profiles of O, H, O$_2$, N$_2$, and the neutral temperature is needed. This is obtained from the MSIS-86 model of *Hedin* [1987]. Figure 1 shows the two neutral atmospheres used for the cases discussed in this paper. The MSIS-86 input conditions used were the following: local time = 1200, Ap = 60, day = 183, magnetic latitude = 74°, magnetic longitude = 180°. For the solar minimum atmosphere a value of 60×10^{-22} W m^{-2} Hz^{-1} was used for $F_{10.7}$ while a value of 190×10^{-22} W m^{-2} Hz^{-1} was used for solar maximum.

In doing each case the model was started with the O$^+$ ionosphere in diffusive equilibrium with $E_c = 0$. At $t = 0$, E_c was changed. In some cases it was abruptly (ramp time = 0) increased to its final value (100 or 200 mV/m) and then held constant through the rest of the run. In other cases, E_c was increased linearly to its final value over a period of several min (3–6). It is likely that the abrupt E_c cases are somewhat unphysical, but they serve to illustrate the maximum effect.

In each run the altitude range (300–1100 km) is divided into 60 cells with about 200,000 simulation ion particles along the whole flux tube. The number of simulation ions is maintained near 200,000 by renormalization as the number of real ions either increases or decreases. (Renormalization is accomplished by either increasing or decreasing all of the simulation particle's normalizations simultaneously and then either eliminating or adding simulation particles to maintain the total content.) The density just below the lower boundary is assumed to be the same as that of the first cell so that whenever an ion leaves the simulation region through the lower boundary a new ion is injected upward there. New ions are continually injected downward through the upper boundary so as to maintain the initial O$^+$ density profile and
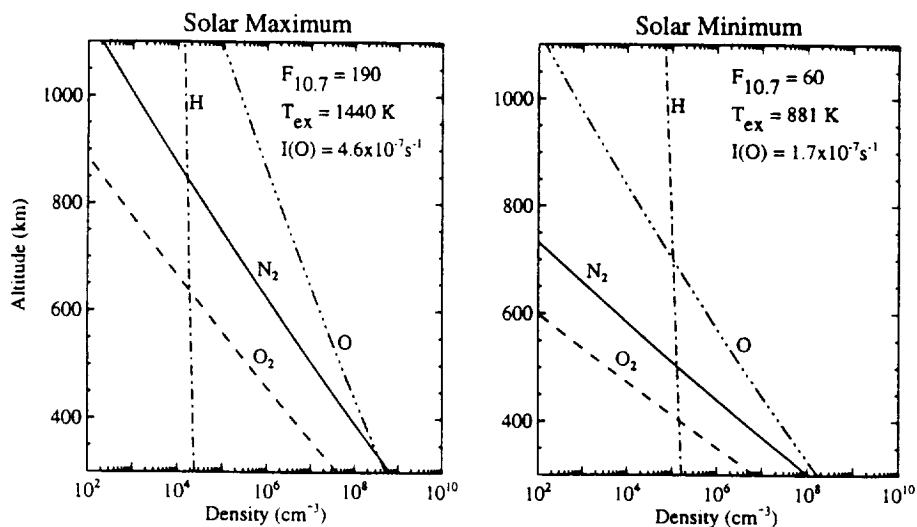
Figure 1. Plots of atomic oxygen, atomic hydrogen, N$_2$ and O$_2$ for the "solar maximum" and "solar minimum" atmospheres used in the model. These profiles come from the MSIS-86 model [*Hedin*, 1987]. A complete listing of the input parameters can be found in the text.

Maxwellian velocity distribution. When ions move upward across the top boundary, they are removed from the simulation. For these reasons, the simulation results are only valid to a point slightly beyond the time when the bulk of the upflowing ions cross the upper boundary. To go much further would require a means of handling ions which cross the upper boundary and then fall back down.

Model results are presented in the form of altitude profiles of bulk parameters (density, drift velocity, flux, parallel temperature, perpendicular temperature, and parallel heat flow) and velocity space contour plots at selected altitudes and times. Bulk parameters were found by appropriate summing of particles in a given cell at a given time, then averaged for 50 time steps. Particles were also summed onto velocity grids (for the velocity space plots) at preselected altitudes and time averaged for either 50 or 100 time steps. During these averaging times the fastest particles seen would travel only about two cells if they experience no collisions.

In doing this type of modeling an important consideration is the size of the time step compared to the various timescales of the problem. Given the densities at 300 km for the solar maximum atmosphere the shortest ion-neutral collision time (for O^+–O polarization and RCE collisions plus O^+–N_2 polarization collisions) is 0.37 s. For the highest O^+ density (1.1×10^5 cm^{-3}) and lowest O^+ temperature (880 K) in the solar minimum cases the shortest self-collision time is 0.37 s. Likewise, for the solar maximum cases the shortest self-collision time is 0.42 s. The shortest chemical reaction time occurs when O^+ is highly heated at low altitudes and is about 15 s for the solar maximum cases with the temperatures which develop in the model results. The longest time step used in these simulations is 0.05 s which is short compared to the smallest of these times. Also, the longest O^+ gyroperiod is 4 ms which is very short compared to the various collision times, thus justifying the gyrotropic assumption.

## 3.　Results for both solar minimum and solar maximum atmospheres

Solar minimum cases

Figure 2 shows bulk parameter time spectrograms for a solar minimum case (with time step $dt = 0.05$ s) where the convection electric field was abruptly increased from 0 to 200 mV/m. The result of this change is seen in all of the moments presented. At $t = 0$ the peak O^+ density is about 1.1×10^5 cm^{-3} at 300 km altitude. Within about 5 min the location of the O^+ peak has moved upward to about 400 km and has dropped in value to about 2×10^4 cm^{-3}. This change is due primarily to enhanced O^+ removal via chemical loss to N_2 and O_2. While this is going on, the O^+ density at higher altitudes is increasing due to the upflow of ions heated above the region where chemical loss is significant. In the parallel velocity panel one can see a velocity pulse traveling upward which obtains a peak speed of about 1.9 km/s near 1000 km after 4 min. The peak flux is about 3×10^9 cm^{-2} s^{-1}, which occurs at a lower altitude and an earlier time.

In the low-altitude ion-neutral collision dominated region the O^+ perpendicular temperature rapidly increases to about 13,000 K as the O^+ velocity distribution becomes toroidal. In the same region, ion-neutral polarization collisions are responsible for an increase of the parallel temperature to about 5000 K. Above the ion-neutral collision dominated region O^+ self-collisions become more important and the the O^+ velocity distribution relaxes toward isotropy. In this region one sees a decline (with altitude) in $T_\perp$ as well as an increase in $T_\parallel$. At higher altitudes, self-collisions decline in importance, and it is possible to develop runaway ions whose velocity is large enough for them to become collisionless. Evidence of this is seen in the large value of the parallel heat flow which is seen to develop near the upper boundary after about 3 min. Figure 3 shows the O^+ velocity distribution at the upper boundary at several times during this period where one can see a nondrifting population and a free streaming population. As the number of upflowing particles increases (the slower ions reach the upper boundary), the free streaming beam merges with the nondrifting population. It is at this time when the maximum upward bulk flow speed is seen at the upper boundary.

Figure 4 shows a few examples of the velocity distributions at the indicated altitudes and times after the convection electric field increase. The distribution function seen at 40 s and at 950 km is an 880 K Maxwellian and is indicative of what is seen at all altitudes before the heating begins. Once heating begins the velocity distribution at the lower boundary (300 km) becomes toroidal very quickly (< 20 s). At higher altitudes (~ 400 km) it takes a bit longer as can be seen. The toroidal distributions do not extend much beyond 400 km in this case since beyond this altitude self-collisions become dominant. Above the toroidal region the velocity distribution attempts to relax to an isotropic form but is not completely successful in doing so. Between 500 and 700 km the distributions maintain a triangular shape indicating a significant amount of upward perpendicular heat flow. Above 800 km the O^+ densities are low enough, initially, so that the newly arriving high speed ions can free stream. Later, the free streaming population merges with the nondrifting ions because of the arrival of slower ions and the large increase in density which causes about a fivefold increase in the self-collision frequency.

In this case one can see three distinct regions which develop and change with time. The low-altitude region is one where ion-neutral collisions dominate. In this region the velocity distribution becomes toroidal and the ion perpendicular temperature is about 3 times higher than the parallel temperature. This is also a region where chemical loss is significant. Above this region ion self-collisions dominate and nearly all traces of the toroidal distribution are lost. However, because of the continued upward flux of ions and energy the distribution does not relax to a Maxwellian. In the third region two distinct ion populations can develop, one streaming relative to the other, for a period of time. The location and extent of these regions will depend on the neutral atmosphere, the initial ion
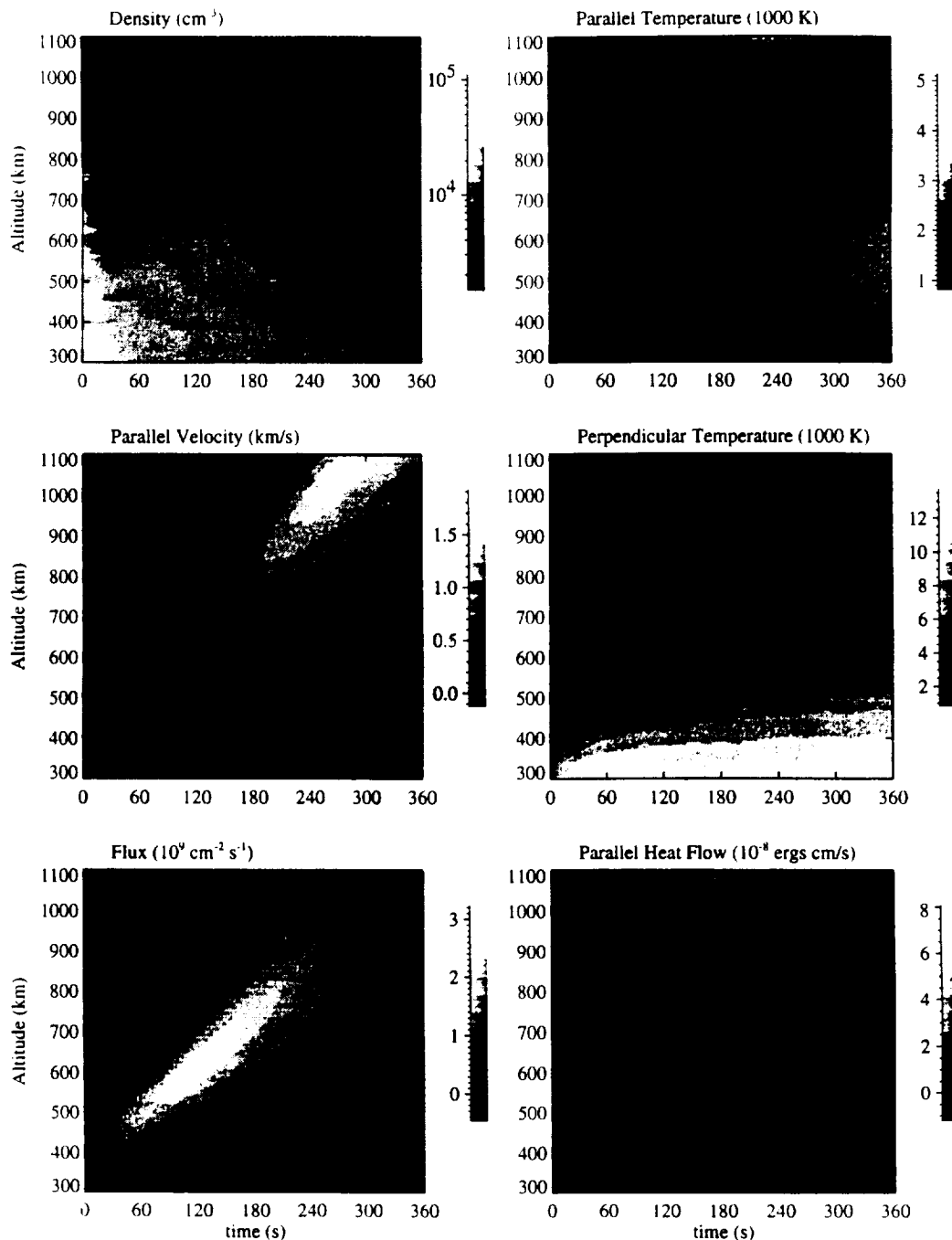
Figure 2. Altitude versus time spectrograms for bulk parameters from case 1 in Table 1. This case used the solar minimum atmosphere from Figure 1 and a convection electric field of 200 mV/m with a ramp time of 0.

densities and the strength of the convection electric field.

The development of the ion free streaming region depends on the strength of the convection electric field and the O$^+$ density profile. For a fast O$^+$ ion moving at a speed u relative to the bulk of the O$^+$ ions its mean free path l is given by

$$l = \frac{2\pi\epsilon_0^2 m^2 u^4}{e^4 n \ln \Lambda} \qquad (7)$$

where m is the ion mass, n is the ion density, and Λ

is the plasma parameter. For an ion density of 3×10^4 cm^{-3} a relative speed (u) of 1 km/s gives a mean free path of only about 1.5 km while a relative speed of ~ 5 km/s gives a mean free path of about 1000 km. When E_c is near 200 mV/m, a significant number of ions are heated to speeds near 5 km/s and, with the O$^+$ densities assumed here, become collisionless with respect to self-collisions. Their increased speed does not give them any advantage with respect to ion-neutral collisions however. The polarization collision mean free path does not change with increasing ion speed,
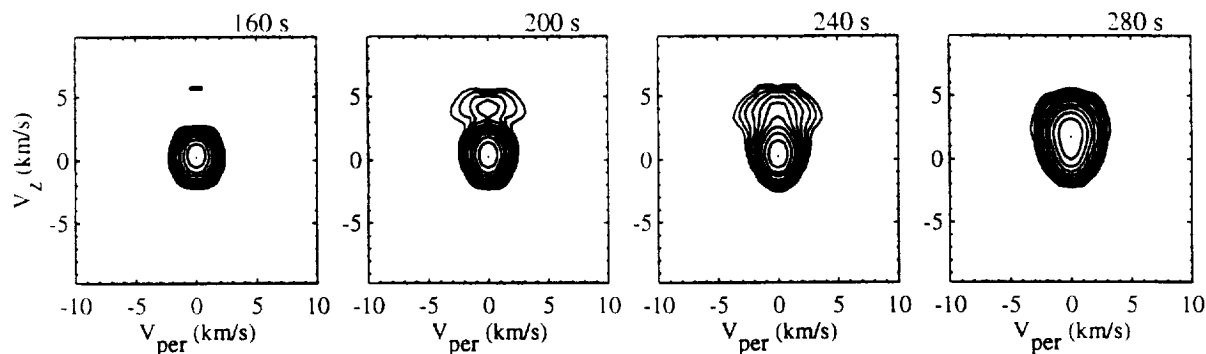
Figure 3. Velocity distributions at 1100 km altitude at the indicated times for case 1 of Table 1 (same as case shown in Figure 2). These distributions are normalized so that their peak value is one and successive contours represent a decrease in the function by a factor of $e^{-1/2}$.
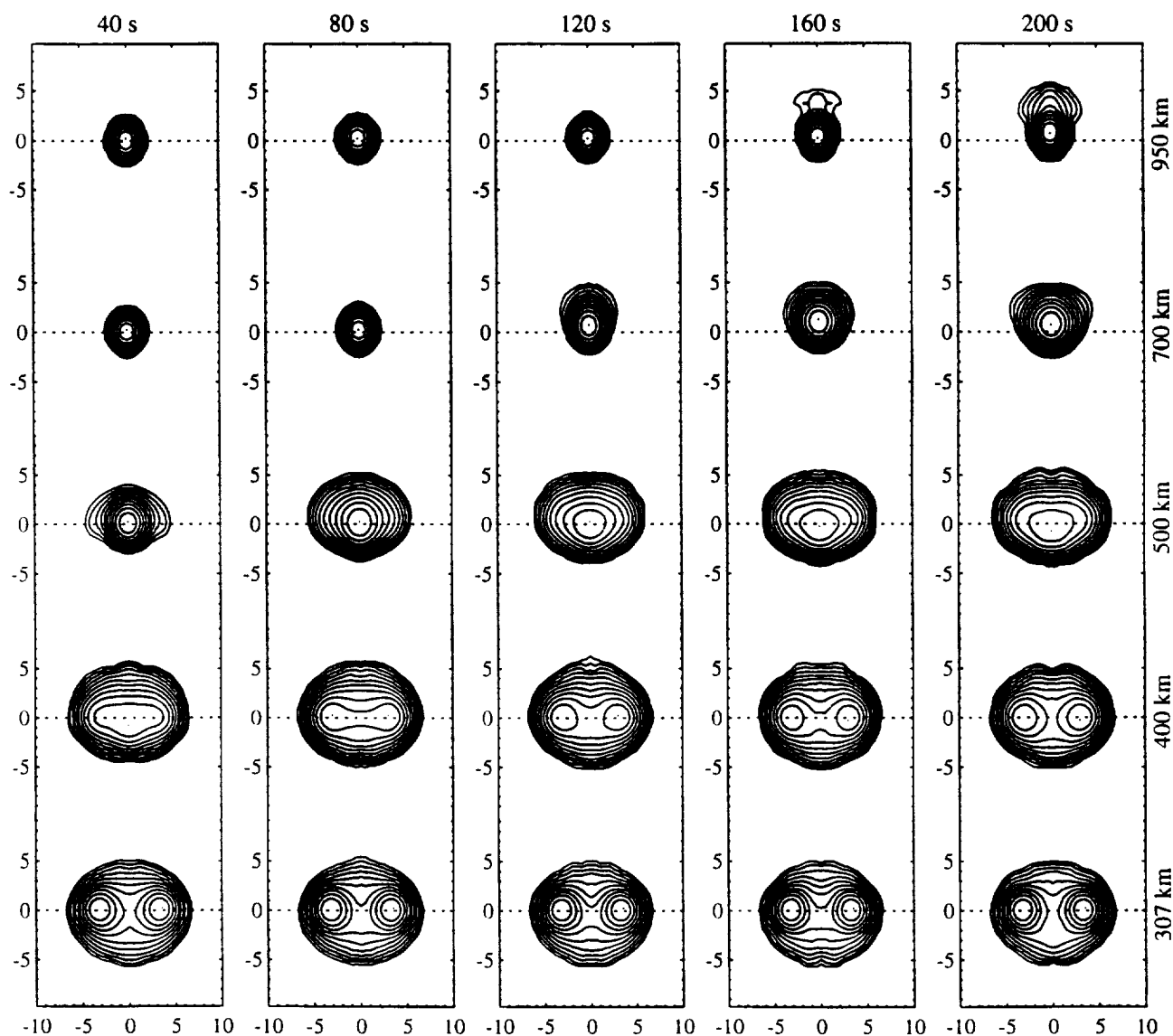
Figure 4. Velocity distributions at the indicated altitudes and times for case 1 of Table 1 (same as case shown in Figure 2). These distributions are normalized so that their peak value is one and successive contours represent a decrease in the function by a factor of $e^{-1/2}$.

while the RCE collision mean free path increases only slightly. To free stream, the ions need to be heated to speeds near 5 km/s, and they must be above the region where ion-neutral collisions dominate. Free streaming is occurring throughout the region above 500 km but does not make a significant contribution to the O$^+$ bulk parameters or velocity distributions unless they are in a region where the O$^+$ density is relatively low. This occurs at altitudes above 850 km before the bulk of the slower moving ions reach that altitude.

A number of other cases were done using the same neutral atmosphere, initial O$^+$ density profile and time step. In the first, E_c is abruptly increased from 0 to 100 mV/m and then held constant. In this case, things develop more slowly than the 200 mV/m case. The peak O$^+$ upward drift speed reaches a value of 0.95 km/s, while the peak flux is 1.8×10^9 cm^{-2} s^{-1}. The maximum perpendicular temperature is about 3800 K and the maximum parallel temperature is about 2500 K. Toroidal velocity distributions do not develop (at least above 300 km). There is also little effect of free streaming since few ions are heated to speeds near 5 km/s. The free streaming velocity distributions seen in Figures 3 and 4 do not develop in this case. The maximum parallel heat flow seen then is about an order of magnitude less than the 200 mV/m case discussed above.

Since the time needed for the effect of the increase in E_c to propagate through the system is only a few minutes, one would expect that when time scales for changes in E_c are on this order the results would change. To see by how much, two cases, in which E_c was increased linearly, were done for comparison. In the first, E_c was increased from 0 to 200 mV/m in 3 min and then ramped back to zero in 3 min. In the second, E_c was increased linearly from 0 to 200 mV/m in 6 min and then held constant. In both of these cases the maximum parallel drift was reduced from 1.9 to 1.4 km/s and the maximum flux was reduced to 2.3×10^9 cm^{-2} s^{-1} for the first case and

to 2.2×10^9 cm^{-2} s^{-1} for the second. The maximum parallel heat flow was reduced to 5.2×10^{-8} ergs cm/s for the first case and to 1.5×10^{-8} ergs cm/s for the second case.

Because of uncertainties in the value of the O$^+$–O RCE collision cross section [*Salah*, 1993] a case was done, similar to the first case discussed above, where this cross section was doubled in value. As a result, the O$^+$ heating rate increases and the region of toroidal distributions expands upward in altitude. The maximum drift speed, flux, and parallel heat flow are all reduce from those seen in case 1. This case, as well as all of the cases discussed above, are summarized in Table 1.

Solar maximum cases

To determine the effect of changing the neutral atmosphere, the cases shown in Table 1 were redone with the solar maximum neutral atmosphere shown in Figure 1. Figures 5 and 6 summarize, in the same way that Figures 2 and 4 do, the results for the solar maximum case which corresponds to case 4 in Table 1. In this case the convection electric field was increased linearly from 0 to 200 mV/m in 6 min and held constant after that. This case uses the same time step used in case 1 of Table 1 (0.05 s). Because of the ramp time things develop more slowly then they do for the case of Figure 1, and one does not see the development of the maximum drift speed and flux until after 6 min. Contrary to what is seen in Figure 1, the maximum parallel heat flow develops near the end of the simulation, after the maximum drift speed has occurred. High perpendicular temperatures occur as high as 700 km altitude where the velocity distribution becomes toroidal near the end of the simulation. At no point in this case do we see distributions where free streaming ions comprise a significant fraction of the total population. This occurs because the long time over which heating is increased provides time for lower-

Table 1. Solar Minimum Cases

Case	t_r, min	E_c, mV/m	V_{max}, km/s	$T_{\perp max}$, K	$F_{\parallel max}$, cm^{-2} s^{-1}	$Q_{\parallel max}$, ergs cm/s
1	0	200	1.9	13,500	3.2×10^9	8.0×10^{-8}
2	0	100	0.95	3,800	1.7×10^9	0.8×10^{-8}
3	3↑ 3↓	200	1.4	13,000	2.8×10^9	5.2×10^{-8}
4	6	200	1.4	13,500	2.2×10^9	1.5×10^{-8}
5*	0	200	1.7	13,700	2.4×10^9	3.5×10^{-8}

*The value $\sigma = 2\sigma_0$ for RCE collisions

Table 2. Solar Maximum Cases

Case	t_r, min	E_c, mV/m	V_{max}, km/s	$T_{\perp max}$, K	$F_{\parallel max}$, cm^{-2} s^{-1}	$Q_{\parallel max}$, ergs cm/s
1	0	200	1.5	15,000	2.2×10^9	4.2×10^{-8}
2	0	100	0.9	4,900	1.3×10^9	0.8×10^{-8}
3	3↑ 3↓	200	1.2	14,400	2.0×10^9	1.7×10^{-8}
4	6	200	1.2	14,400	1.8×10^9	2.0×10^{-8}
5*	0	200	1.2	15,000	1.3×10^9	2.3×10^{-8}
6*	0	100	0.75	4,700	0.9×10^9	0.9×10^{-8}

*The value $\sigma = 2\sigma_0$ for RCE collisions
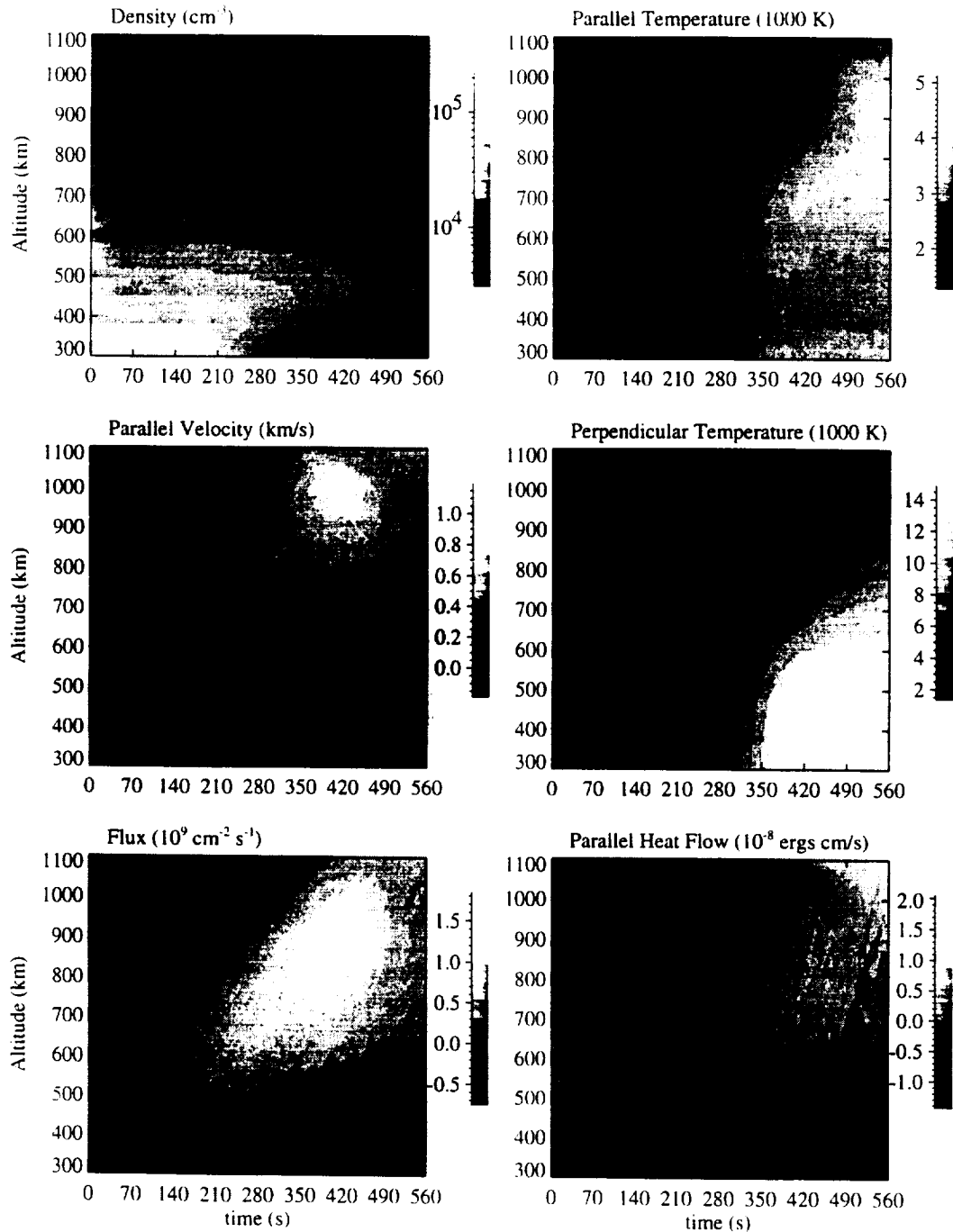
Figure 5. Altitude versus time spectrograms for bulk parameters from case 4 in Table 2. This case used the solar maximum atmosphere from Figure 1 and a convection electric field of 200 mV/m with a ramp time of 6 min.

speed ions, heated early, to reach higher altitudes before the higher-speed ions, heated later, can. At late times in this simulation the O⁺ velocity distribution is toroidal from 300 km to 700 km above which it has a predominately triangular shape due mainly to the upflow of perpendicular energy.

Table 2 summarizes several cases done with the solar maximum atmosphere shown in Figure 1. In comparing with the solar minimum cases one can see that the maximum perpendicular temperatures are slightly higher while the maximum parallel drift speed,

flux, and heat flow are all lower. This difference is due to the greater extent of the region where ion-neutral collisions dominate. Although the higher neutral densities produce greater heating rates, they also are responsible for a greater frictional force which leads to reduced drift speeds and fluxes. At altitudes above 1100 km one would see, for a solar maximum atmosphere, the development of larger parallel drift speeds and heat flows as one more fully enters the free streaming region where ion-neutral collisions are negligible.
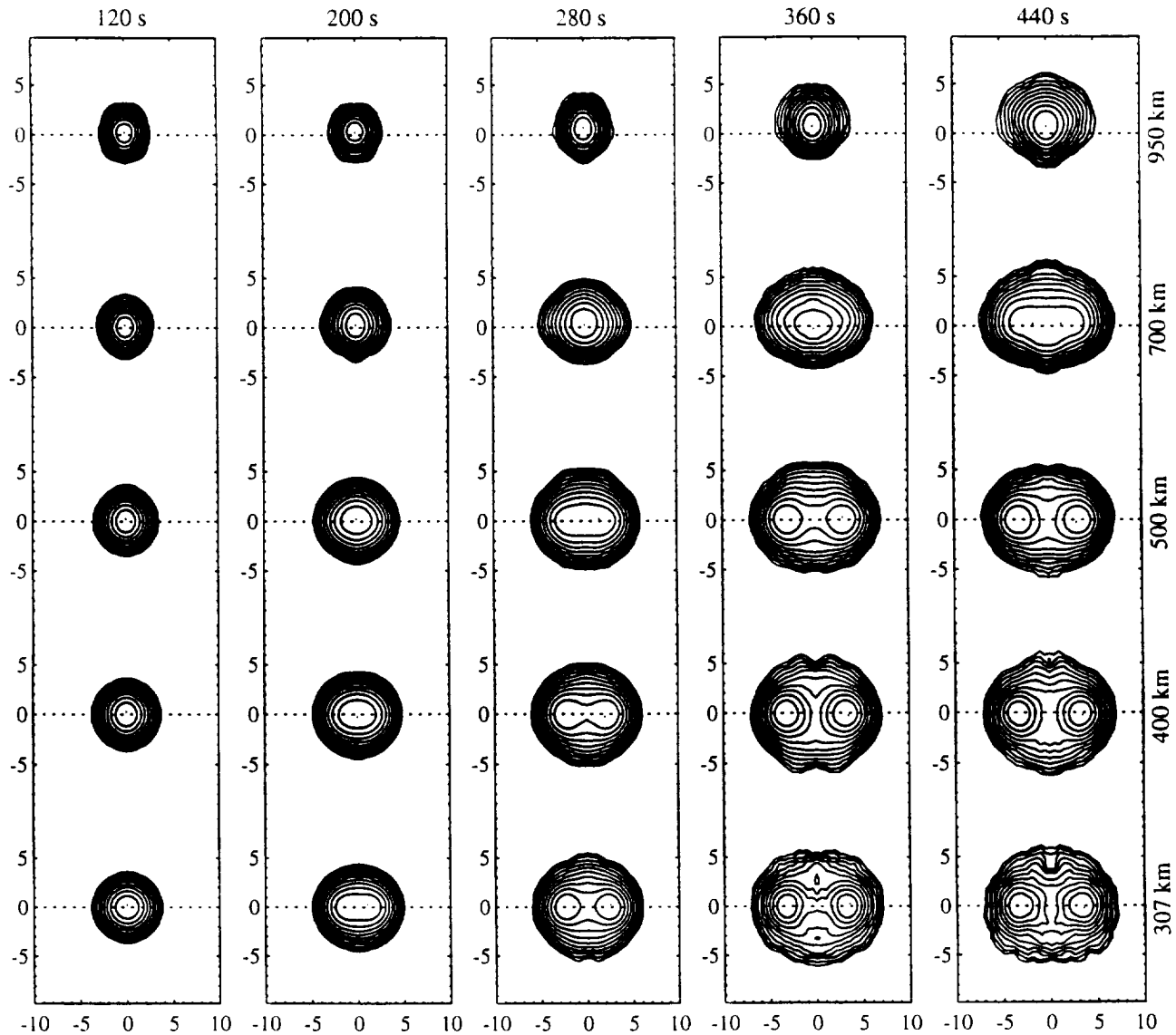
Figure 6. Velocity distributions at the indicated altitudes and times for case 4 of Table 2 (same as case shown in Figure 5).

In the various solar minimum and solar maximum cases presented above, free streaming ions, ions which are upflowing and essentially collisionless with respect to self-collisions, are produced whenever O$^+$ ions are energized to speeds above 4 km/s. Whether or not they make a significant contribution to the total ion population (below 1000 km) such that they have an impact on bulk parameters such as parallel heat flow or temperature, depends on the neutral atmosphere scale height and on the time history of the convection electric field. Those cases for which this happens are the solar minimum cases 1, 3, and 5, and the solar maximum case 1. The presence of significant numbers of free streaming ions occurs, in these model results, whenever the parallel per particle heat flow ($h_\parallel$) exceeds about 2.5×10^{-8} ergs cm/s or where the ratio

$$\frac{h_\parallel}{kT_\parallel \sqrt{kT_\parallel/m}} \tag{8}$$

exceeds 0.5. (For case 1 in Table 1 the maximum value of this ration is about 1.2.) Each of the cases where this happens are ones where the convection electric field increases to its final value fairly rapidly (in less than 3 min). It is also more likely to happen when the neutral atmosphere is cooler since ion-neutral collisions become insignificant at lower altitudes. Also, lower O$^+$ densities make it more likely for ions to free stream because of the reduced self-collision frequency. Each time the ratio in 7 exceeds 0.5 the velocity distribution is characterized by a separate upflowing O$^+$ population or an extended superthermal tail.

4. Discussion

From the results in this paper we can make the following general conclusions about what will happen to the topside ionosphere whenever the convection electric field increases from a small value ($<$ 25 mV/m)

to a large value (100–200 mV/m) in 6 min or less. At altitudes below 1000 km the upward parallel drift will peak at values between 500 m/s and 2 km/s, the parallel flux peaks at values between 6.0×10^8 and 3.2×10^9 cm^{-2} s^{-1}, and the parallel per particle heat flow peaks at values between 8.0×10^{-9} and 8.0×10^{-8} ergs cm/s. The higher values in these ranges occur for a cooler atmosphere and a larger convection electric field that is turned on rapidly.

Before comparing these results with previous modeling work it is helpful to understand an issue central to this topic. During periods of rapid $\mathbf{E} \times \mathbf{B}$ drift the ions are heated primarily in the perpendicular direction via RCE collisions with atomic oxygen. In order to develop upflows this perpendicular energy must be converted to parallel energy. The mirror force is a candidate for performing this conversion; however, because of the relatively large magnetic field scale length it cannot produce strong upflows over the distances involved here. Another candidate process is the ambipolar electric field, but in these simulations the electron temperature remains uniform and constant, while the plasma density gradient decreases so that the electric potential drop along the field line actually decreases with time. As such, this force makes a decreasing contribution to the upflows seen. O$^+$–neutral polarization collisions and O$^+$–O$^+$ self-collisions can transfer perpendicular energy to parallel energy but, of themselves, cannot impart upward momentum to the ions (assuming the neutrals have no vertical drift). They can produce elevated parallel temperatures at low altitude which greatly enhances the preexisting parallel pressure gradient and which in turn drives the upflows.

To test the contribution of the two isotropizing collision processes on the development of upflows, case 1 of Table 1 was redone, once with both polarization and self-collisions turned off and once with only self-collisions turned off. O$^+$–O RCE collisions were turned on in both cases. In the first of these two cases an upsurge of O$^+$ ions did develop; however, its maximum parallel velocity was 870 m/s, its maximum flux was 9.1×10^8 cm^{-2} s^{-1} and the maximum parallel heat flow was 3.3×10^{-9} ergs cm/s. Because of the lack of self-collisions, toroidal free streaming populations began to flow up through the existing nondrifting Maxwellian population but these free streaming ions only attained a parallel flow speed of about 2–3 km/s compared to the 4–5 km/s of the free streaming populations seen in case 1 of Table 1. When only self-collisions were turned off, a much stronger upflow developed. In this case the maximum parallel velocity was 1.5 km/s, the maximum flux was 1.7×10^9 cm^{-2} s^{-1} and the maximum parallel heat flow was 6.6×10^{-8} ergs cm/s. In this case, free streaming populations with drift speeds of 4–5 km/s developed which were similar to those seen in Figure 3, except that they were broader in the perpendicular velocity direction, and they showed no tendency to merge with the existing population as occurs in the last plot in Figure 3.

The results of these last few cases clearly illustrate the importance of isotropizing collisions for the development of O$^+$ upflows that result from $\mathbf{E} \times \mathbf{B}$ frictional heating. Since these upflows are primarily pressure gradient driven flows the magnitude of the upflow will depend on the rate at which the pressure gradient increases. This increase rate depends on the ion heating rate and the efficiency with which polarization and self-collisions isotropize the distribution. Polarization collisions act primarily at low altitude in the region where ion-neutral collisions dominate, while self-collisions are important mainly above this region. In the strong convection cases, one might think that the heating of the ions in the low altitude ion-neutral collision dominated region would leave them energetic enough so that they are collisionless to the point where isotropization via self-collisions would be inefficient. However, when ions are nearly collisionless, there exists an intermediate stage where the ions do not exchange much energy with each other but their velocity vectors are easily deflected. As such, the self-collision process can remain fairly efficient at isotropizing the distribution, particularly just above the ion-neutral collision dominated region where O$^+$ densities are still high. Kinetic details of how these collisions operate become important to the overall upflow story.

Prior to initiation of ion heating the O$^+$ pressure profile is such that the ions are in hydrostatic equilibrium. Once heating begins this equilibrium is upset and pressure transport begins to relax the increased pressure gradient. Pressure transport is accomplished in two ways. One is the transmission of the pressure upward in a diffusive process through self-collisions. The second method is through the free streaming of nearly collisionless energetic ions which introduces the effect of velocity dispersion into the results. Both of these pressure relaxation processes operate simultaneously in these simulations.

Differences or similarities of the results in this paper and the results from previous work will have much to do with the isotropization issue and the ion free streaming issue. The model used in the works of *Sellek et al.* [1991], *Moffett et al.* [1991], and *Heelis et al.* [1993] assumed an isotropic O$^+$ temperature so that the issue of transfer of perpendicular to parallel energy is side stepped since the ions are directly heated in the parallel direction. Our results differ significantly from those produced by the isotropic hydrodynamic model. For cases in the present paper where the maximum convection speed is 2 km/s ($E_c = 100$ mV/m) and is turned on instantaneously, the maximum O$^+$ upflow speed is only about 0.9 km/s compared to values twice as large from the hydrodynamic results. This difference may be due to the smaller O$^+$ parallel temperature which develops in the semikinetic model and to differences in the temperature versus altitude profile from the two models. The semikinetic model produces upflow velocities as large as 1.9 km/s, but only for convection speeds near 4 km/s and for atmospheric conditions near solar minimum. Also, in our results we see greater upflow speeds and fluxes for solar minimum conditions than for solar maximum conditions. This is opposite to what is seen in the isotropic hydrodynamic results.

In the paper by *Körösmezey et al.* [1992] cases with higher convection electric fields (150 and 200 mV/m) were done. The model employed was a 20-moment

generalized transport model [*Gombosi and Rasmussen.* 1991], which allows for temperature anisotropy and parallel and perpendicular heat flow. One of the results of their calculations is that the maximum upward drift speed does not exceed 400 m/s for altitudes below 1000 km. This conclusion is significantly different from ours where the maximum upward drift speed can approach 1.5 km/s for similar convection electric field strengths in a solar maximum atmosphere. Several things may explain this difference. In the *Körösmezey et al.* calculations the convection electric field is turned on with a 10-min ramp time compared to our maximum ramp time of 6 min. In comparing cases 1 and 4 in Table 2 one can see that increasing the ramp time decreases the maximum drift speed. Another difference is that we assumed a uniform electron temperature of 2000 K, while they had a steep electron temperature increase (from the neutral exospheric temperature to about 4400 K) over the 200 to 1000 km altitude range. (This electron temperature profile is probably more appropriate for an open rather than a closed flux tube because of the assumed downward electron heat flow imposed at the upper boundary.) This will reduce the ambipolar electric field and reduce somewhat the upflow speeds. In order to make a better comparison we performed a case with the same ramp time and electron temperature profile. A neutral atmosphere at solar maximum. 2400 LT and at a latitude corresponding to an L shell of $L = 5$ was also used. In this case the parallel drift speed near 1100 km reached a value of about 750 m/s by the end of the 10-min ramp time and a maximum value of 800 m/s 30 s later. It appears that kinetic effects (free streaming ions and isotropization) accounts for the remaining differences between the results of these two model types.

In the results of *Sellek et al.* [1991], *Moffett et al.* [1991], *Heelis et al.* [1993] and *Körösmezey et al.* [1992] the O⁺ drift speeds which develop at low altitudes (< 500 km) are downward with magnitudes of 50 to 200 m/s. These downflows are the result of O⁺ chemical loss at low altitude and the shifting of the F2 peak to higher altitude. In our results we see basically the same thing: downwards flows of 50–200 m/s below 500 km. All of these results contrast sharply with the results of *Anderson et al.* [1991] where large upward ion velocities were seen at low altitude in SAID events.

Above about 500 km, for cases done with the solar minimum atmosphere in Figure 1 and a 200 mV/m convection electric field, our results compare favorably with those of *Loranc and St-Maurice* [1994], at least as far as the drift velocity is concerned. The parallel and perpendicular temperature versus altitude profiles are however, significantly different; we see more structure in the parallel temperature and a larger perpendicular temperature gradient. Much of this difference is due to self-collisions and the fact that most of energy given to the ions in the friction heating process goes into perpendicular motion resulting in larger temperature anisotropies than are assumed in the Loranc and St-Maurice model. For the solar maximum cases we see more differences with lower drift speeds at high altitudes and greater temperature anisotropies at the exobase. Many of the abrupt changes in the

velocity distribution function seen in their results are smoothed out or eliminated in our results because of collisions. From our results we concluded that above an altitude of about 900 km the Loranc and St-Maurice model probably gives resonable results since ion-neutral collisions are insignificant there and O⁺ are low enough so that ions streaming with a speed of only 2–3 km/s would be collisionless.

Our results compare well with some of the observations. First, the parallel drift speeds and fluxes produced in the model (with convection electric fields in the 50–200 mV/m range) fall in the same range as those of the thermal ion upwelling events studied by *Tsunoda et al.* [1989] using HILAT data. Second, the flow velocities and parallel temperatures seen in the 100 mV/m cases compare favorably with what is seen in a typical "type 1" event discussed by *Wahlund et al.* [1992]. We also develop higher drift speeds (> 1 km/s) as are seen in the "type 2" events, but only with convection electric fields greater than 150 mV/m. In none of our results do we get parallel drift speeds as high as 3 km/s which is seen for upward drifts in some radar data [*Yeh and Foster*, 1990] and satellite data [*Loranc et al.*, 1991]. If most of the upflow in those data are field-aligned then some other process, such as electron precipitation. might need to be invoked to account for the higher flow speeds. As previously noted, we do not see large parallel drift speeds at low altitude as reported by *Anderson et al.* [1991]

References

Albritton, D. L., I. Dotan, W. Lindinger, M. McFarland, J. Tellinghuisen. and F. C. Fehsenfeld, Effect of ion speed distributions in flow-drift tube studies of ion-neutral reactions, *J. Chem. Phys.*, 66, 410, 1977.

Anderson, P. C., R. A. Heelis, and W. B. Hanson, The ionospheric signatures of rapid subauroral ion drifts, *J. Geophys. Res.*, 96, 5785. 1991.

Banks. P. M., and G. Kockarts, *Aeronomy*, Academic, San Diego, Calif., 1973.

Barakat, A. R., and R. W. Schunk, O⁺ions in the polar wind, *J. Geophys. Res.*, 88, 7887, 1983.

Barakat, A. R., R. W. Schunk, and J.-P. St-Maurice, Monte carlo calculations of the O⁺ velocity distribution in the auroral ionosphere. *J. Geophys. Res.*, 88, 3237, 1983.

Cannata, R. W., T. L. Killeen, T. I. Gombosi, A. G. Burns and R. G. Roble. Modelling of time-dependent ion outflows at high geomagnetic latitudes, *Adv. Space Res.*, 8, 89, 1988.

Gombosi, T. I., and T. L. Killeen, Effects of thermospheric motions on the polar wind: A time-dependent numerical study, *J. Geophys. Res.*, 92, 4725, 1987.

Gombosi, T. I., and C. E. Rasmussen, Transport of gyration-dominated plasmas of thermal origin, 1, Generalized transport equations, *J. Geophys. Res.*, 96, 7759, 1991.

Hedin, A. E., MSIS-86 thermospheric model, *J. Geophys. Res.*, 92, 4649, 1987.

Heelis, R. A., G. J. Bailey, R. Sellek, R. J. Moffett, and

B. Jenkins, Field-aligned drifts in subauroral ion drift events, *J. Geophys. Res., 98,* 21,493, 1993.

Keating, J. G., F. J. Mulligan, D. B. Doyle, K. J. Winser, and M. Lockwood, A statistical study of large field-aligned flows of thermal ions at high-latitudes, *Planet. Space Sci., 38,* 1187, 1990.

Knof, H., E. A. Mason, and J. T. Vanderslice, Interaction energies, charge exchange cross sections, and diffusion cross sections for N⁺-N and O⁺-O collisions, *J. Chem. Phys., 40,* 3548, 1964.

Körösmezey, A., C. E. Rasmussen, T. I. Gombosi and G. V. Khazanov, Anisotropic ion heating and parallel O⁺ acceleration in regions of rapid **E×B** convection, *Geophys. Res. Lett., 19,* 2289, 1992.

Kozyra, J. U., T. E. Cravens, and A. F. Nagy, Energetic O⁺ precipitation, *J. Geophys. Res., 87,* 2481, 1982.

Loranc, M., and J.-P. St-Maurice, A time-dependent gyrokinetic model of thermal ion upflows in the high-latitude *F* region, *J. Geophys. Res.,* in press, 1994.

Loranc, M., W. B. Hanson, R. A. Heelis, and J.-P. St-Maurice, A morphological study of vertical ionospheric flows in the high-latitude *F* region, *J. Geophys. Res., 96,* 3627, 1991.

Millward, G. H., S. Quegan, R. J. Moffett, T. J. Fuller-Rowell, and D. Rees, A modelling study of the coupled ionospheric and theromospheric response to an enhanced high-latitude electric field event, *Planet. Space Sci., 41,* 45, 1993.

Moffett, R. J., R. Sellek, and G. J. Bailey, The behavior of H⁺ and He⁺ ions in the topside ionosphere during a short-lived subauroral ion drift, *Planet. Space Sci., 39,* 1209, 1991.

Providakes, J., and C. E. Seyler, Collisional electrostatic ion cyclotron waves as a possible source of energetic heavy ions in the magnetosphere, *J. Geophys. Res., 95,* 3855, 1990.

St-Maurice, J.-P., and R. W. Schunk, Ion velocity distributions in the high-latitude ionosphere, *Rev. Geophys., 17,* 99, 1979.

Salah, J. E., Interim standard for the ion-neutral atomic oxygen collision frequency, *Geophys. Res. Lett., 20,* 1543, 1993.

Schunk, R. W., and A. F. Nagy, Ionospheres of the terrestrial planets, *Rev. Geophys., 18,* 813, 1980.

Schunk, R. W., and J. C. G. Walker, Ion velocity distributions in the auroral ionosphere, *Planet. Space Sci., 20,* 2175, 1972.

Schunk, R. W., W. J. Raitt, and P. M. Banks, Effect of electric fields on the dayside high-latitude *E* and *F* regions, *J. Geophys. Res., 80,* 3121, 1975.

Sellek, R., G. J. Bailey, R. J. Moffett, R. A. Heelis, and P. C. Anderson, Effects of large zonal plasma drifts on the subauroral ionosphere, *J. Atmos. Terr. Phys., 53,* 557, 1991.

Singh, N., K. S. Hwang, D. G. Torr, and P. Richards, Temporal features of the outflow of heavy ionospheric ions in response to a high altitude plasma cavity, *Geophys. Res. Lett., 16,* 29, 1989.

Takizuka, T., and H. Abe, A binary collision model for plasma simulation with a particle code, *J. Comput. Phys, 25,* 205, 1977.

Torr, M. R., and D. G. Torr, Energetic oxygen: A direct coupling mechanism between the magnetosphere and thermosphere, *Geophys. Res. Lett., 6,* 700, 1979.

Tsunoda, R. T., R. C. Livingston, J. F. Vickrey, R. A. Heelis, W. B. Hanson, F. J. Rich, and P. F. Bythrow, Dayside observations of thermal-ion upwellings at 800-km altitude: An ionospheric signature of the cleft ion fountain, *J. Geophys. Res., 94,* 15,277, 1989.

Wahlund, J.-E., H. J. Opgenoorth, I. Häggström, K. J. Winser, and G. O. L. Jones, EISCAT observations of topside ionospheric ion outflows during auroral activity: Revisited, *J. Geophys. Res., 97,* 3019, 1992.

Wilson, G. R., Semikinetic modeling of the outflow of ionospheric plasma through the topside collisional to collisionless transition region, *J. Geophys. Res., 97,* 10,551, 1992.

Wilson, G. R., C. W. Ho, J. L. Horwitz, N. Singh, and T. E. Moore, A new kinetic model for time-dependent polar plasma outflow: Initial results, *Geophys. Res. Lett., 17,* 263, 1990.

Winkler, E., J.-P. St-Maurice, and A. R. Barakat, Results from improved Monte Carlo calculations of auroral ion velocity distributions, *J. Geophys. Res., 97,* 8399, 1992.

Yeh, H.-C., and J. C. Foster, Storm time heavy ion outflow at mid-latitude, *J. Geophys. Res., 95,* 7881, 1990.

G. R. Wilson, Center for Space Plasma and Aeronomic Research, EB-136M, The University of Alabama in Huntsville, Huntsville, AL 35899. (e-mail: cspar::wilsong or wilsong@cspar.uah.edu)